Buoyant disruption of magnetic arcades with self-induced shearing

Ward Manchester IV[1]

High Altitude Observatory, National Center for Atmospheric Research, Boulder, Colorado, USA
Department of Astronomy, University of Illinois, Urbana, Illinois, USA

Received 7 January 2002; revised 24 October 2002; accepted 20 December 2002; published 26 April 2003.

[1] We present the results of magnetohydrodynamic (MHD) simulations of the nonlinear development of instabilities of magnetically sheared arcades and show how they relate to plasmoid ejections and coronal mass ejections (CMEs). To model the arcade disruptions, we capitalize on a family of analytical solutions for initial states; these describe magnetic arcades in uniform gravity that are characterized by magnetic shear. Two-and-a-half-dimensional (2.5-D) time-dependent simulations were performed with the ZEUS-2D code to show the response of the arcades to small velocity perturbations. The model arcades respond by rising and expanding, and most significantly, we find shearing motions naturally arise in conjunction with the instability. This field line shearing is in response to the Lorentz force, which drives large-amplitude Alfvén waves, which in turn transport magnetic shear from the lower to the upper extremities of the arcades. The self-induced shear Alfvén waves, coupled with magnetic buoyancy, provide a feedback mechanism that drives the arcades to a loss of equilibrium and disruption following a long period of slow rise and expansion. These simulations of arcade disruptions may be relevant with regard to CME initiation for three major reasons. First, the arcade disruptions are the result of undriven magnetic buoyancy instabilities. Second, magnetic field line shearing is an intrinsic aspect of the instability that occurs spontaneously and is driven only by the magnetic tension force. (No imposed shear motions are specified.) Third, the arcade disruption process has been found to repeat without prompting. *INDEX TERMS:* 7871 Space Plasma Physics: Waves and instabilities; 7524 Solar Physics, Astrophysics, and Astronomy: Magnetic fields; 7509 Solar Physics, Astrophysics, and Astronomy: Corona; 7519 Solar Physics, Astrophysics, and Astronomy: Flares; 7513 Solar Physics, Astrophysics, and Astronomy: Coronal mass ejections; *KEYWORDS:* magnetohydrodynamics, Sun, instabilities, coronal mass ejection

Citation: Manchester, W., IV, Buoyant disruption of magnetic arcades with self-induced shearing, *J. Geophys. Res.*, *108*(A4), 1162, doi:10.1029/2002JA009252, 2003.

1. Introduction

[2] Coronal mass ejections (CMEs) have traditionally been defined as large-scale expulsions of plasma from the corona seen as bright arcs in coronagraphs that record Thomson scattered light. These events are the most stunning activity of the solar corona in which typically $10^{15}-10^{16}$ g of plasma is hurled into interplanetary space with a kinetic energy of the order $10^{31}-10^{32}$ ergs. Extensive observations with the SMM coronagraph have shown that many CMEs originate from the disruption of large-scale coronal structures known as helmet streamers [*Hundhausen*, 1987, 1993]. A more recent study of Large-Angle and Spectrometric Coronagraph (LASCO) images has found that 63 percent of CMEs are related to pre-existing streamers while 35 percent are unrelated [*Subramanian et al.*, 1999]. Helmet streamers are arcade-like structures commonly found in coronagraph images to possess a three part structure composed of a high density shell covering a low density cavity at the base of which lies a filament. That many CMEs originate from helmet streamers is strongly suggested by the appearance of many CMEs possessing a dense bright leading shell with a cavity containing a bright core which can be interpreted as the corresponding three-part structure of the pre-event helmet streamer as shown by *Hundhausen* [1999], *Howard et al.* [1997], and *Gibson and Low* [1998]. It is now believed that the breakup of helmet streamers is the likely result of a loss of equilibrium following a slow nearly quasi-static evolution [*Low*, 1983]. A slow growth followed by eruption is consistent with the observations of the swelling and brightening of large coronal helmet streamers several days before they produce CMEs [*Hundhausen*, 1993].

[3] Of central importance to the structure and evolution of helmet streamers is their magnetic field, about which much can be inferred from both theory and observations. For a

[1]Now at Department of Atmospheric, Oceanic, and Space Sciences, University of Michigan, Ann Arbor, Michigan, USA.

0148-0227/03/2002JA009252

helmet streamer to be in static equilibrium, the underlying magnetic field must be in a closed configuration to confine the dense plasma that would otherwise be carried out with the solar wind. Observations show that the photospheric magnetic field associated with helmet streamers is in a bipolar configuration where opposite polarities are largely separated by a neutral line. Furthermore, in the corona, X-ray loops are clearly found to coincide with the helmet streamers, indicating a dominant loop-type magnetic configuration [*Sterling and Hudson*, 1997]. A significant feature of the field configurations associated with CMEs is magnetic shear which is observed at the photosphere [*Wang*, 1992] with vector magnetograms and is strongly suggested in the corona by the presence of X-ray sigmoids [*Moore et al.*, 2001]. Thus, the magnetic field configuration of pre-event helmet streamers is very likely a sheared arcade, which may also contain a flux rope as suggested by *Low* [1994] and *Low and Hundhausen* [1995] coinciding with the plasma cavity. It is believed that CMEs are the result of a global magnetohydrodynamic (MHD) process and represent a significant restructuring of the global coronal magnetic field [*Low and Hundhausen*, 1987; *Low*, 1996].

[4] The outstanding goal of CME research is to determine the mechanism by which the pre-event coronal structures erupt. Early theories of initiation suggested that thermal pressure associated with solar flares was the driving mechanism [*Dryer et al.*, 1979]. However, this model fell from favor when observations revealed that flares often occur after CME initiation. It is now believed that only the solar magnetic field is capable of driving CMEs. Most magnetic-driven models of CMEs have employed pre-event coronal magnetic fields in closed configurations that are either potential or force-free. The potential field has zero free energy while the force-free field has been shown by *Aly* [1991] and *Sturrock* [1991] to possess less energy than the open state, greatly limiting its ability to erupt. To induce an eruption from such magnetic states, two primary mechanisms have been invoked. First, localized magnetic reconnection has been selectively introduced to sever field lines and relieve magnetic tension to allow a portion of the system (typically a flux rope) to expand rapidly upwards. Examples of reconnection driven CMEs models are those by *Forbes and Priest* [1995], *Lin and Forbes* [2000], and *Chen and Shibata* [2000]. Second, a combination of system driving and magnetic reconnection has been used to model the initiation of CMEs. In the most common example, magnetic arcades are made to approach an open state by way of prescribed footpoint motions that shear the magnetic field. Reconnection when applied within the shearing arcade results in eruption. For examples of such models, see *Wolfson* [1982], *Mikić et al.* [1988], *Steinolfson* [1991], *Choe and Lee* [1996], *Mikić and Linker* [1994], and *Linker and Mikić* [1995]. *Antiochos et al.* [1999] have produced a new variation of this model employing a quadrapole field, which allows magnetic reconnection to occur higher in the corona, which removes the unsheared field above a low-lying sheared core.

[5] In our work, we have chosen a different approach to modeling CMEs. To begin with, our model for the pre-event coronal structure is a bipolar arcade in magnetostatic equilibrium with the weight and pressure of the surrounding stratified plasma. This configuration allows the system to contain substantial free energy and circumvents the constraint of *Aly* [1991] and *Sturrock* [1991] by virtue of a nonzero cross-field component of the electric current. The equilibrium states possessing these properties are members of a family of two-dimensional (2D) analytical solutions derived by *Low and Manchester* [2000] (hereinafter referred to as LM) which describe an isothermal atmosphere embedded with sheared magnetic arcades. Here we find that the evolution of these arcades to eruption proceeds as an ideal MHD instability that is initiated by only a small velocity perturbation. The time-dependent behavior of the arcades is modeled with two-and-a-half-dimensional (2.5D) ideal MHD numerical simulations performed with the ZEUS-2D code.

[6] Our numerical models of arcade eruptions are significant for three reasons. First, the evolution of these arcades occurs fundamentally as undriven ideal MHD instabilities. When magnetic reconnection occurs in our models by numerical diffusion, it does so as a secondary effect well after the arcade eruption is under way. Second, magnetic field line shearing is an intrinsic aspect of the instability that spontaneously occurs and is driven by the magnetic tension force. No shearing motions are imposed. The tension force drives large-amplitude shear Alfvén waves that transport magnetic flux to the expanding portion of the arcade. Finally, in one particular simulation, the eruption process repeats from a single structure with no prompting other than the initial velocity perturbation.

[7] The remainder of the paper is organized in the following fashion. Details of the initial states are given in section 2 while the results of the simulations are presented in section 3. In the latter section, we explore the physical processes guiding the evolution of the arcades and show that a powerful feedback mechanism exists between magnetic buoyancy and self-induced shearing that drives the arcades to erupt. In section 4, we relate the evolution of the model arcades to the observed behaviors of pre-event helmet streamers, CMEs and post-eruption X-ray arcades. Finally, in section 5, we discuss the results of the simulations and their significance in demonstrating an initiation mechanism for CMEs and plasmoid ejections.

2. Governing Equations of MHD and Initial States

[8] To model the MHD instabilities of sheared arcades discussed herein, we assume that the systems are composed of magnetized plasma that behaves as an ideal gas with a polytropic index, $\gamma = \frac{5}{3}$. The plasma is taken to have infinite electrical conductivity so that the magnetic field is frozen to the plasma. The gravitational acceleration, g, is constant in the negative z direction [we use Cartesian coordinates (x, y, z)]. With these assumptions, the evolution of the system is governed by the following ideal MHD equations:

$$\frac{\partial \rho}{\partial t} + \nabla \cdot (\rho \mathbf{v}) = 0 \tag{1}$$

$$\rho\left(\frac{\partial \mathbf{v}}{\partial t} + (\mathbf{v} \cdot \nabla)\mathbf{v}\right) = -\nabla p + \frac{1}{4\pi}(\nabla \times \mathbf{B}) \times \mathbf{B} - \rho g \hat{z} \tag{2}$$

$$\frac{\partial e}{\partial t} + \nabla \cdot (e\mathbf{v}) = -p(\nabla \cdot \mathbf{v}) \tag{3}$$

$$p = (\gamma - 1)e \tag{4}$$

$$\frac{\partial \mathbf{B}}{\partial t} = \nabla \times (\mathbf{v} \times \mathbf{B}) \tag{5}$$

where ρ is the mass density, p is the plasma pressure, e is the internal energy density (per unit volume), $\mathbf{v}$ is the velocity field and $\mathbf{B}$ is the magnetic field. The simulations are invariant in the x direction so that $\left(\frac{\partial}{\partial x}\right) = 0$. However, we allow for non-zero velocity and magnetic field components in all three directions.

2.1. Sheared Magnetostatic Arcades of LM

[9] For our simulations, we employ members of a LM family of magnetostatic isothermal atmospheres as initial states. These equilibria are analytic solutions of the force balance equation

$$\frac{1}{4\pi}(\nabla \times \mathbf{B}) \times \mathbf{B} - \nabla p - \rho g \hat{z} = 0, \tag{6}$$

and Maxwell's equation, $\nabla \cdot \mathbf{B} = 0$, that describe magnetic arcades in force balance with the pressure and weight of the surrounding plasma. The arcades are translationally invariant along the x axis and sheared by a nonzero B_x component. The solutions are periodic in the y direction and vertically, the field lines of the arcades extend to $z \rightarrow -\infty$. Within an arcade, there exists a density-depleted cavity in which the magnetic pressure compensates for reduced plasma pressure and a downward directed magnetic tension force offsets the buoyancy of the cavity. These solutions also have the property that any given amount of magnetic flux may be freely distributed over a system of field lines that are of fixed geometry. This freedom allows us to truncate the magnetic field of the solution by prescribing that the field strength go to zero on a given field line, and then filling all remaining space with field-free plasma. In this way we have chosen to accommodate a single arcade in a computational domain that would otherwise contain several Fourier cells. Finally, we should mention that these equilibria offer advantages over simpler potential and force-free magnetic arcades that have often been used in past studies. Foremost, the magnetostatic solutions allow magnetic buoyancy to play an essential role in the instabilities that lead to the ultimate disruption of the arcades.

[10] We briefly describe here the mathematical form of the LM solutions. More complete derivations and descriptions of the solutions can be found by *Low and Manchester* [2000]. The solutions depend on only two spatial coordinates, y and z, in which case the magnetic field can be written in terms of two scalar functions A and B_x,

$$\mathbf{B} = \left(B_x, \frac{\partial A}{\partial z}, -\frac{\partial A}{\partial y}\right), \tag{7}$$

a form that automatically satisfies $\nabla \cdot \mathbf{B} = 0$. Solutions to equation (6) for 2D atmospheres have the property that B_x is a strict function of A. Force balance along field lines, subject to the ideal gas law and isothermal condition,

$$p = \frac{k}{m}\rho T_0, \tag{8}$$

demands that the plasma pressure be of the form

$$p = P(A)\exp\left(-\frac{z}{H}\right), \tag{9}$$

to ensure equilibrium. Here m, k, and T_0 are, respectively, the mean molecular mass, the Boltzmann constant, and the constant temperature, in terms of which the pressure scale height takes the form, $H = kT_0/gm$.

[11] Mathematically, the LM solutions are defined in terms of a flux coordinate, $\phi(y, z)$, that has the form

$$\phi = \exp\left(-\frac{z}{2H}\right)\cos(qy). \tag{10}$$

The magnetic field, $\mathbf{B}$, is defined in terms of $A(\phi)$, and $B_x(\phi)$ by the equation,

$$\mathbf{B} = \left(B_x(\phi), \frac{dA}{d\phi}\frac{\partial \phi}{\partial z}, -\frac{dA}{d\phi}\frac{\partial \phi}{\partial y}\right), \tag{11}$$

where $B_x(\phi)$ is of the form

$$B_x^2(\phi) = \lambda + \left(q^2 - \frac{1}{4H^2}\right)\phi^2\left(\frac{dA}{d\phi}\right)^2 \tag{12}$$

necessary to satisfy the x component of the force balance equation (6).

[12] For this family of solutions, members are distinguished by the flux function $A(\phi)$ and by the horizontal spatial frequency, q, used in defining ϕ. The functional form of $A(\phi)$ and the value of q may be freely chosen with only the restriction that q be sufficiently large that B_x^2 is positive. With this mathematical construction, the expression for plasma pressure may be written as

$$p = P(\phi)\exp\left(-\frac{z}{H}\right), \tag{13}$$

where $P(\phi)$ takes the form

$$P(\phi) = P_0 - \frac{q^2}{8\pi}\left(\frac{dA}{d\phi}\right)^2. \tag{14}$$

2.2. Initial Conditions

[13] The model 1 coronal arcade is defined by the flux coordinate, given by equation (10), with $q = 1/H$. The flux function, $A(\phi)$, is taken to have the form

$$A(\phi) = \frac{B_0 H\left(\phi_0 - 4\phi^2\right)}{8\phi^4}. \tag{15}$$

This particular choice of $A(\phi)$ produces physically desirable features in the initial state. First, it allows the magnetic field to go smoothly to zero on the field line defined by $\phi = \sqrt{\phi_0/2}$. Beyond this line, we place an isothermal field-free atmosphere in pressure balance with the arcade. Second, this construction spatially isolates a single magnetic arcade placed away from the vertical boundaries of the computational domain, which, in turn, minimizes the boundaries' influence on the nonlinear dynamics modeled

in the simulations. For these selections, the magnetic arcade solution takes the form:

$$B_x = \frac{\sqrt{3}}{2} B_0 \frac{(2\phi^2 - \phi_0)}{2\phi^4} \tag{16}$$

$$B_y = -\frac{1}{2} B_0 \frac{(2\phi^2 - \phi_0)}{2\phi^4} \tag{17}$$

$$B_z = B_0 \exp\left(-\frac{z}{2H}\right) \sin\left(\frac{y}{H}\right) \frac{(2\phi^2 - \phi_0)}{2\phi^5} \tag{18}$$

$$P(\phi) = P_0 - \frac{B_0^2}{8\pi} \frac{(2\phi^2 - \phi_0)^2}{4\phi^{10}}. \tag{19}$$

[14] For the model 2 photosphere-type initial state, the flux coordinate, given by equation (10), is defined with $q = 2/H$. The flux profile, $A(\phi)$, is taken to have the form given by

$$A(\phi) = B_0 H \frac{(\phi_0 - 2\phi)}{2\phi^2}. \tag{20}$$

This choice of ϕ and $A(\phi)$ produces a sheared magnetic arcade in pressure balance with a field-free atmosphere similar to model 1. However, the arcade in this case is distinguished by a field strength that falls off more slowly with depth, and for a given pressure scale height, H, the arcade is half as wide as that of model 1. For this choice of q and $A(\phi)$, the arcade solution takes the form:

$$B_x = \frac{\sqrt{15}}{2} B_0 \frac{(\phi - \phi_0)}{\phi^2} \tag{21}$$

$$B_y = -\frac{1}{2} B_0 \frac{(\phi - \phi_0)}{\phi^2} \tag{22}$$

$$B_z = 2B_0 \exp\left(-\frac{z}{2H}\right) \sin\left(\frac{2y}{H}\right) \frac{(\phi - \phi_0)}{\phi^3} \tag{23}$$

$$P(\phi) = P_0 - \frac{B_0^2}{2\pi} \frac{(\phi - \phi_0)^2}{\phi^6}. \tag{24}$$

[15] The parameters chosen to completely specify the (model 1) coronal equilibrium state are as follows: $\phi_0 = 0.5$, $B_0 = 0.73$ Gauss, $T_0 = 1.0 \times 10^6$ K, and $\rho_0 = 1.0 \times 10^{-15}$ g cm^{-3}. The (model 2) photospheric system is defined with $\phi_0 = 0.5$, $B_0 = 3500$ Gauss , $T_0 = 6.0 \times 10^3$ K, $\rho_0 = 3.3 \times 10^{-6}$ g/cm^3. In both cases, we assume uniform gravity with $g = 2.734 \times 10^4$ cm s^{-2} and $m = 1.3 m_h$ where m_h is the molecular weight of hydrogen. The physical parameters defined above introduce length, velocity and time scales that characterize the equilibrium states and the dynamics of the instabilities exhibited by the systems. For the model 1 system, the scales have values of $H = 2.3 \times 10^9$ cm, $c_s = 8.0 \times 10^6$ cm s^{-1} and $\tau = H/c_s = 290$ s. For the much cooler photospheric system, the values are $H = 1.40 \times 10^7$ cm, $c_s = 6.18 \times 10^5$ cm s^{-1} and $\tau = H/c_s = 22.6$ s. The minimum plasma β's for the coronal and photospheric arcades are 0.41 and 0.86 respectively.

[16] Profiles of the magnetic field strength as a function of height through the centers of the coronal and photospheric arcades are shown in Figures 1a and 1b, respectively, while the density stratification for the models are shown in Figures 1c and 1d. Examining the density, we see that magnetic field lines of the arcades enclose cavities of low-density plasma. Force balance is established by the magnetic pressure, replacing the plasma pressure lost by the density depletion, while the downward magnetic tension force is offset by the buoyancy of the cavity. This non-force-free configuration sets the stage for the positive feedback between the buoyancy and self-induced shearing that will ultimately lead to the disruption of the arcades.

[17] In LM, it was shown that the arcade solution is stable provided that $q^2 < \frac{1}{4H^2}$. Clearly then, the initial states do not satisfy the condition for stability, still determination of the particular mode of instability and its growth rate remains outside the scope of this research. To date, stability analysis of magnetic arcades has been restricted to force-free configurations in which the affects of plasma pressure, density and gravity are neglected [*Kusano and Nishikawa*, 1996]. The inclusion of plasma pressure, especially in the form of a gravitationally stratified atmosphere, will certainly change the behavior of the system compared to a force-free state.

2.3. Numerical Procedures and Boundary Conditions

[18] The simulations detailed here were performed with the ZEUS-2D code, which is made available to the astrophysical community by the Laboratory for Computational Astrophysics (LCA) at the National Center for Supercomputing Applications (NCSA). Developed by *Stone and Norman* [1992a, 1992b], the ZEUS-2D code explicitly solves the equations of ideal (nonresistive, nonviscous, adiabatic), non-relativistic MHD, including applied and self gravity, as well as radiation transport. ZEUS-2D is an Eulerian finite difference code that uses the method of characteristics to resolve and properly advect magnetic tangential discontinuities, while shocks are resolved with the use of artificial viscosity as shown by *Richtmyer and Morton* [1967]. The code employs the Van Leer monotonic upwind advection scheme to give precise material advection. This advection technique is one aspect of the operator splitting employed by the ZEUS-2D code where the advection (transport) and body forces (source) terms in a given equation are handled independently. The tests and accuracy of the ZEUS-2D code have been described by *Stone and Norman* [1992a, 1992b]. For the simulations presented here, we compile ZEUS-2D strictly for ideal MHD, choosing the option to evolve the component of the velocity field, v_x, that is in the invariant direction.

[19] The computational domain for model 1 extends from $z_{min} = -3.3 \times 10^9$ cm to a height $z_{max} = 5.0 \times 10^{10}$ cm and in the horizontal direction, extends for $|y| < 1.0 \times 10^{10}$ cm. The grid configuration is non-uniform Cartesian to provide

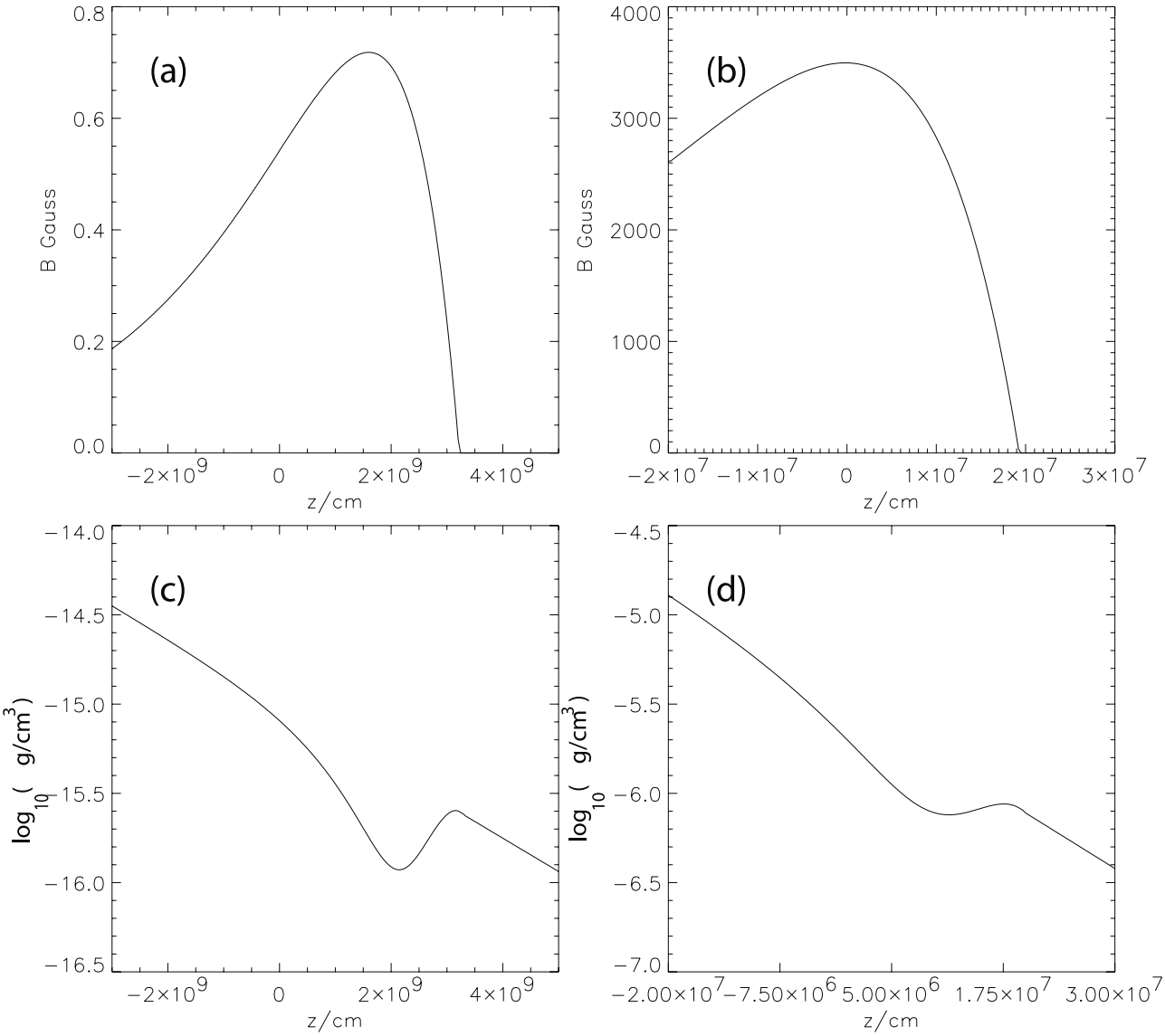

Figure 1. The magnetic field strengths of the initial-state coronal and photospheric arcades are plotted as a function of height, z, through the centers of the arcades and are shown in frames (a) and (b) respectively. In both cases, the field strength rise and falls off gently, reaching a zero value on field lines prescribed by $\phi = \phi_0$ and $\phi = \sqrt{(\phi_0/2)}$ for the photospheric and coronal magnetic arcades respectively. Similar plots of the vertical density structure for the coronal and photospheric models (frames c and d, respectively) reveal that buoyant cavities exist inside each arcade where the plasma density is reduced by as much as a factor of 4 compared to the ambient atmosphere. In both cases, the arcades are surrounded by isothermal field-free plasma.

high resolution of the initial state. In the vertical direction, 170 uniformly spaced grid points are in the interval $-3.5 \times 10^9 < z < 3.5 \times 10^9$ cm and 150 grid points in the interval $3.5 \times 10^9 < z < 5.0 \times 10^{10}$ cm. In the top interval, the distance between grid points expands with height by a factor of 1.01 between successive points. In the horizontal direction, there are a total of 60 points the two intervals $1.0 \times 10^{10} < |y| < 4.0 \times 10^9$ cm, 180 points in the intervals $4.0 \times 10^9 < |y| < 1.0 \times 10^9$ cm and 120 points in the interval $|y| < 1.0 \times 10^9$ cm. The grid points are highly focused in the horizontal direction at the center of the domain to provide high resolution of the current sheet that forms at the time of eruption. This delays the onset of magnetic reconnection, which will be shown to be significant to the energetics of the eruption.

[20] The domain for model 2 extends from $z_{min} = -2.0 \times 10^7$ cm to $z_{max} = 6.0 \times 10^7$ cm and extends horizontally for $|y| < 2.0 \times 10^7$ cm. In the vertical direction, 150 grid points are evenly distributed between $-2.0 \times 10^7 < z < 2.0 \times 10^7$ cm while 50 points are evenly spread over the upper half of the domain. In the horizontal direction, 200 points are evenly distributed. It should be noted that the $z = 0$ axis of each model is not to be identified with a particular height in the atmosphere such as the photosphere. Rather $z = 0$ is only significant with regard to the analytical expressions that define the initial states. The density at the base of

Model 1 is 5.0×10^{-15} g cm^{-3}, consistent with the transition region, while the base of Model 2 at a density of 1.25×10^{-5} g cm^{-3} is 3.5 pressure scale heights below the photosphere.

[21] Boundary conditions are taken to be periodic at $y = y_{min}$ and $y = y_{max}$, and with an outflow boundary at $z = z_{max}$, which allows waves to exit the system. The bottom boundary at $z = z_{min}$ is designed to be nonpenetrating in the z direction while allowing diffusive motions in the horizontal directions y and x. To be precise, the boundary condition at $z = z_{min}$ is established by fixing the pressure, density and the magnetic field strength in the ghost cells to the analytical values of the initial equilibrium state. In the ghost cells, the velocity v_z is reflected (same magnitude, opposite sign as the adjacent active grid point) while v_x and v_y are set to zero. Motion at this boundary between the ghost cells and active cells is prescribed by averaging the velocities across the interface. The bottom boundary is very diffusive and dampens horizontal motions propagated from the interior, no shearing motions are imposed. The resisted horizontal motion is meant to emulate the arcades connection below to a denser more slow moving atmosphere. The nonpenetrating nature of the boundary is chosen to prevent mass loss.

3. Results of Numerical Simulations

[22] In this section, we present the results of two 2.5-D numerical simulations designed to study the nonlinear disruption of sheared magnetic arcades resulting from MHD instabilities. The first simulation addresses instabilities and the disruption of a coronal arcade embedded in a million degree plasma. The physical scale of the resulting eruption can be convincingly compared to plasmoid ejections observed to occur in arcades over-lying sheared portions of photospheric neutral lines. The second simulation addresses a smaller arcade in the photosphere where a plasma β close to unity is more consistent with observed plasma densities and field strengths. We also use a different magnetic flux profile in this case to determine how the instability might depend on arcade structure as well as the physical regime in which the arcade is placed. Together, the simulations will be shown to demonstrate a flux transport mechanism that not only explains the initiation and driving of larger scale CMEs, but also self-consistently explains events observed to proceed CMEs, such as increased magnetic shear and arcade swelling.

3.1. Results of Model 1

[23] To initiate the growth of an instability, the coronal arcade is given a velocity perturbation of the mathematical form

$$v_z = v_0 \cos\left(\frac{y}{2H}\right) \exp\left(-\frac{4|z - z_c|}{H}\right). \quad (25)$$

Here, the amplitude is $v_0 = 0.08 c_s$, and z_c is calculated so that the perturbation is centered vertically on the topmost field line of the magnetic arcade. The imposed velocity is confined horizontally to a narrow region centered on the arcade for which $|y| < (\pi H/8)$.

[24] Figure 2 shows the time evolution of the magnetic field in a sequence of images for times t = 0.0, 6.25, 6.67, 7.08, 7.50, 7.91, 8.30, 8.75 hr. This figure depicts the magnetic field projected on the y-z plane as black lines superposed on a false color image of the angle between the magnetic field and the plane of variation. The first frame shows the initial state of the arcade. Here, we see that the magnetic field is least sheared at the footpoints (approximately 30 degrees from the plane of variation) and grows more sheared with height, reaching nearly 60 degrees at the crest. In response to the perturbation, the coronal loop rises very slowly for a period of approximately 8 hr (= 100 τ). During this phase of evolution, the upper portion of the arcade (delineated by 6 field lines) expands and rises while the lower arcade remains nearly motionless. Examination of the false color image of Figure 2 reveals that the expanding portion of the magnetic field has grown increasingly sheared even though no shearing motions are *imposed* at the footpoints. By t = 7.91 hr, the arcade is found rapidly erupting and by t = 8.30 hr the field lines of the narrow portion of the arcade begin to reconnect. By the last frame at t = 8.75 hr, reconnection has completely severed the erupting portion of the arcade into an isolated flux rope ejected into the field-free atmosphere. We point out that the minor asymmetries in the final frame are the result of discretization errors in the numerical scheme that only become manifest after magnetic reconnection.

[25] A plot of the log (base 10) of the kinetic energy as a function of time as shown in Figure 3 reveals much about the growth of the instability and the disruption of the arcade. As it evolves, the energy (shown as a solid black line) first exhibits a short lived and sporadic increase. This growth can be attributed to the finite resolution of the numerical mesh, which causes departures from equilibrium in the initial state. The system takes 1.5 hr to settle down at which point the kinetic energy begins to grow exponentially for a period of 5.5 hr with an e-folding time of approximately 5 hr. Following this long period of growth, the arcade's sudden eruption occurs with a super-exponential growth of the kinetic energy lasting approximately two hours. The final peak in kinetic energy occurs with the onset of magnetic reconnection after which the kinetic energy begins to decay. The dashed line of Figure 3 shows the kinetic energy of a simulation identical in every way to model 1, except that motions in the x direction are artificially suppressed. In this case, the arcade is stable indicating that self-induced shearing motions are essential for the growth of the instability.

[26] There are clearly three distinct phases of evolution for the arcade. The first phase of evolution is characterized by a nearly quasi-static adjustment of forces to keep the structure in approximate equilibrium. There is slow (although exponential) growth in the kinetic energy as the arcade rises at velocities that are of order 1 percent the sound speed as seen in Figure 4. This development persists for approximately 50 Alfvén transit times until the arcade grows increasingly distended so that by t = 7.91 hr, it suddenly erupts upwards, making the transition to a second phase of evolution. The eruption occurs as a loss of equilibrium that takes place on a time scale of 5 Alfvén transit times and is characterized by a super-exponential growth of kinetic energy and rise velocities that exceed the sound speed (see Figure 4). By 8.0 hr into the simulation, field lines in the neck of the arcade pinch together through processes of ideal MHD to suddenly form a current sheet.

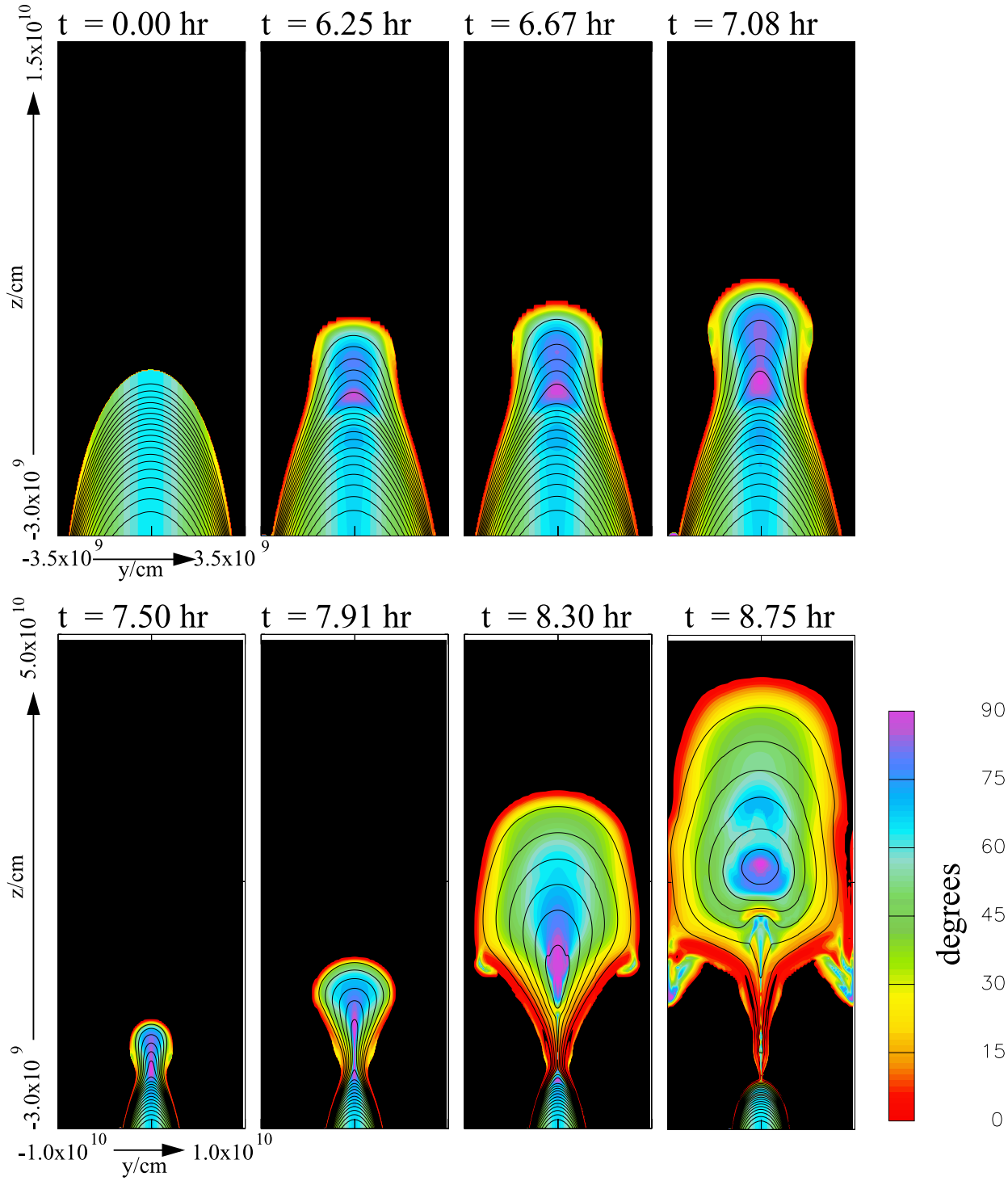

Figure 2. Results for the coronal model. Depicted is a time sequence of images showing the evolution of the magnetic field of the coronal arcade for times $t = 0.0$, 6.25, 6.67, 7.08, 7.50, 7.91, 8.30, and 8.75 hr. The magnetic field is displayed as field lines projected on the y-z plane in black and the shear angle measured between the field lines and the plane of variation is shown in false color. The evolution occurs very slowly as the field lines in the upper part of the arcade begin to expand upwards and spontaneously shear, turning toward the direction of invariance. The top four frames show an expanded view that clearly shows the formation of a highly sheared core in the arcade that appears as a purple colored region forming at the loop crests. The arcade continues to rise very slowly for a period of 7 hours and grows increasingly more sheared as it does so. The arcade then reaches a critical point where it looses equilibrium and erupts very suddenly in the last 40 minutes of the simulation. In the final frame, we see that magnetic reconnection severs the upper arcade to form a flux rope that is ejected from the system. Notice that the sheared core separates the field lines that erupt from those that do not.

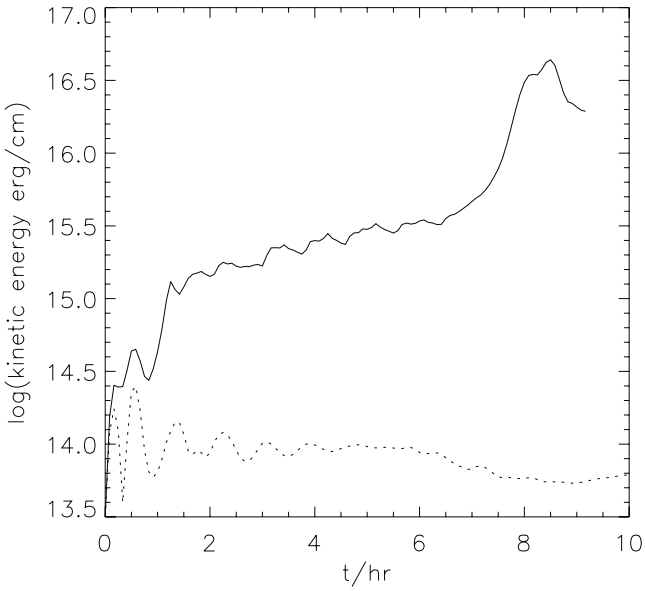

Figure 3. Log (base 10) of the kinetic energy of the coronal arcade and surrounding atmosphere are shown as a function of time given by the solid black line. The dashed line depicts the kinetic energy of an identical system with the exception that all motions out of the plane of variation have been artificially suppressed. In both cases, the initial perturbation energy is of the order of $10^{13.5}$ ergs/cm. When spontaneous shearing motions are allowed, we find that the kinetic energy grows roughly exponentially for a period of 7 hours followed by a 1 hour period in which the energy grows at a super-exponential rate, coinciding with the arcade eruption. With restricted motions, the kinetic energy oscillates and decays, indicating the necessity for shearing motions for the growth of the instability.

The third phase of evolution is distinguished by the development of a tearing-mode instability and magnetic reconnection at the current sheet. The reconnection process is controlled by numerical diffusion, which may be interpreted to mimic resistive magnetic reconnection without Joule heating. For this model, the magnetic diffusivity is greatly minimized at the current sheet owing to the dense concentration of grid points there.

[27] It is clear from Figure 2 that the magnetic field becomes increasingly sheared in the expanding portion of the arcade as it rises to greater heights. To make the point more clear, in Figure 5a, we show the shape of a single magnetic field line of the arcade as seen from two perspectives, seen projected on the *y*-*z* plane as a solid line, and on the *x*-*y* plane as a dashed line. The time sequence of the field line projected on the *x*-*y* plane shows graphically how the field line is sheared and drawn parallel to the direction of invariance, which corresponds to the neutral line beneath the arcade. At the same time the field line in the legs of the arcade becomes more nearly perpendicular to the direction of invariance. This shearing happens as the footpoints of the arcade spontaneously move in opposite directions. As the arcade balloons at times $t = 7.91$, 8.30 hr, the field line takes on a distinct sigmoid shape. The last frame shows the field line of the arcade after it has undergone magnetic reconnection to eject a flux rope. In the process, magnetic shear is significantly reduced in the reconnected field line of the arcade. It is important to note that none of the shearing motions are imposed but rather occur self-consistently as an essential aspect of the MHD instability.

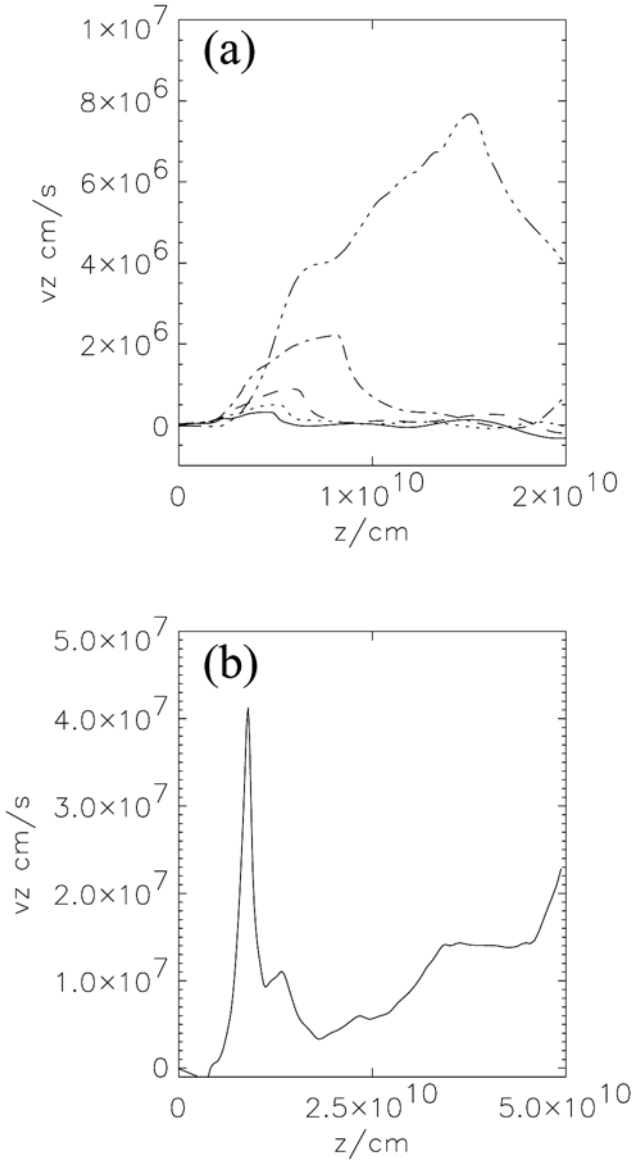

Figure 4. The vertical velocity, v_z, is plotted as a function of height through the center of the erupting coronal arcade. Five curves are drawn in Figure 4a, showing the velocity at times $t = 6.25$, 6.67, 7.08, 7.50, and 7.91 hr as solid, dots, dashes, dot-dash and dash-dot-dot-dot lines respectively. During the pre-eruption expansion, the rise velocity is only a few percent of the sound speed and the velocity profile increases in a nearly self-similar fashion. Figure 4b shows the velocity near the peak of the eruption ($t = 8.30$ hr). Here we find the upper portion of the magnetic loop rising at 140 km s^{-1} while a reconnection jet is clearly evident in the neck of the arcade. The jet consists of plasma shooting upwards at 400 km s^{-1} which drives an MHD shock into the forming flux rope as shown in Figure 11.

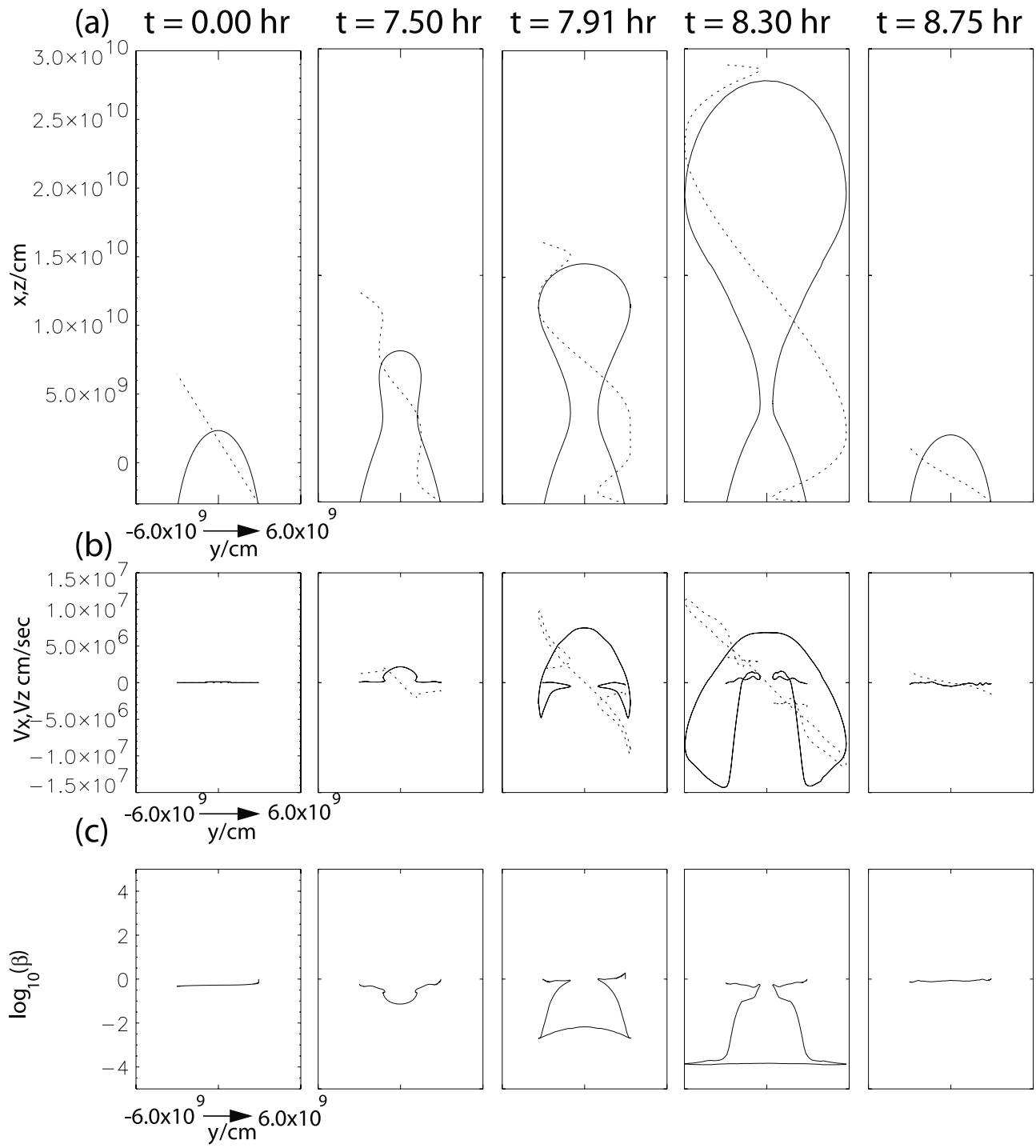

Figure 5. Depicted are evolutionary sequences of the coronal arcade for times t = 0.0, 7.50, 7.91, 8.30, and 8.75 hr. Figure 5a shows the evolution of a single field line of the system as seen projected on the y-z plane as a solid line and projected in the x-y plane as a dashed line. Figure 5b shows the velocity of the plasma located on the field line depicted in Figure 5a. The vertical (v_z) component is shown as a solid line while the shear (v_x) component is shown as a dashed line. Figure 5c shows the plasma β along the magnetic field line depicted in Figure 5a.

[28] Figure 5b shows the velocity of the plasma located on the field line shown in Figure 5a. The vertical component, v_z, is shown as a solid line while the shear component, v_x is shown as a dashed line. The vertical component shows the center of the field line rising at speeds as high as 80 km s^{-1} at time t = 7.91 while strong downflows occur at the sides of the loop. At later times, the downflow velocity exceeds the rise velocity, reaching speeds of -150 km s^{-1} at time t = 8.30 hr. In the sequence of images, the shear velocity (v_x) is clearly seen to be greatest when the arcade is

most rapidly expanding. The highest shear velocity occurs in a narrow region at the widest part of the expanding loop and reaches a magnitude exceeding 100 km s^{-1}. The shear velocity rapidly decreases with depth so that the footpoints never shear at a rate greater than 20 km s^{-1}. Finally, the last row of plots of Figure 5c shows the plasma β along the same field line. In the initial state, the plasma β is at a nearly constant value of 0.5 along the entire length of the field line. As the arcade slowly expands into the exponentially stratified atmosphere, the plasma β drops off rapidly and reaches a minimum of 0.03 by time t = 7.50 hr. When the arcade finally erupts, the plasma β falls dramatically to 10^{-4} along the upper dome of the expanding loop while the β of the legs of the arcade remains largely unaffected.

3.2. Analysis of Magnetic Shear

[29] Here, we describe the magnetic shearing quantitatively and explain the reason for it with simple physical arguments. To begin, it is important that we explicitly define the magnetic field components as they apply to both the simulations and observations of the sun. We will always use the terms longitudinal and transverse to apply to field components as they are observed at the solar limb, which corresponds to the plane of variation of our 2.5D simulations. In this case, the longitudinal component is parallel to the direction of invariance in the simulations and is denoted as B_x. In the solar context, this field component is along the solar surface and is parallel to the magnetic neutral line. The transverse component is in the plane of variation of the simulation, and its magnitude is given by $B_T = \sqrt{B_y^2 + B_z^2}$.

[30] As was previously shown by *Manchester* [2001] the time evolution of the magnitudes of the longitudinal and transverse field components behave very differently in 2.5D geometry. As the instability develops, the transverse field behaves much as one would expect from the expansion and compression field lines in the plane of variation. However, the longitudinal field, rather than becoming weak in the expanding loop and remaining strong in the arcade legs, tends instead to evolve to a constant value along the entire length of the field line. The reason for this behavior of the longitudinal field was first demonstrated by *Manchester and Low* [2000] and is the result of the Lorentz force and the nature of force balance in the direction of the invariance. Our system possesses 2-D variations and a field component, B_x, along the ignorable coordinate. If we look at the x component of equation (6), we note that the only force results from the bending of magnetic field lines and may be written as

$$F_x = \frac{1}{4\pi}\left[\frac{\partial B_x}{\partial y}\frac{\partial A}{\partial z} - \frac{\partial B_x}{\partial z}\frac{\partial A}{\partial y}\right] = \frac{1}{4\pi}\nabla B_x \cdot \mathbf{B_T}. \qquad (26)$$

Clearly, for there to be no force out of the plane, B_x must be a constant along a field line. This result is an unavoidable property of symmetric magnetostatic configurations, possessing a field component along the direction of invariance. If B_x is not constant along a field line, then the unbalanced Lorentz force will cause shearing motions in the direction of invariance.

[31] Examination of the induction equation demonstrates how such shearing motions affect the longitudinal component of the field, B_x, during the evolution of the system. The induction equation is

$$\frac{\partial \mathbf{B}}{\partial t} = \nabla \times (\mathbf{v} \times \mathbf{B}) \qquad (27)$$

of which the x component may be written as

$$\frac{\partial B_x}{\partial t} + \nabla \cdot (B_x \mathbf{v}) = \frac{\partial}{\partial y}(v_x B_y) + \frac{\partial}{\partial z}(v_x B_z). \qquad (28)$$

The left-hand side of equation (28) expresses the continuity of B_x as it is advected in the y-z plane. The right-hand side of the equation can be thought of as a source term, which results from the shearing of the transverse field in the x-direction.

[32] In the simulation of the instability, the plasma motion associated with the expanding arcade not only bends the transverse field but also advects the longitudinal component, B_x. Such an expansive motion weakens the longitudinal field in the loop, as shown in Figure 6. This figure shows the transverse field strength (dashed line) and the longitudinal field, (solid line) B_x plotted as a function of distance along an arcade field line at t = 8.0 hours. Here, we see that there is a clear gradient in B_x that results in a Lorentz force in the direction of invariance. We notice that as we travel along the field line from right to left, in the direction of **B**, the gradient in B_x is negative as we ascend the arcade, zero near the field line crest, and positive as we descend the field line. Consequently, the Lorentz force points in the $+x$ to $-x$ directions on the left and right hand sides of the arcade

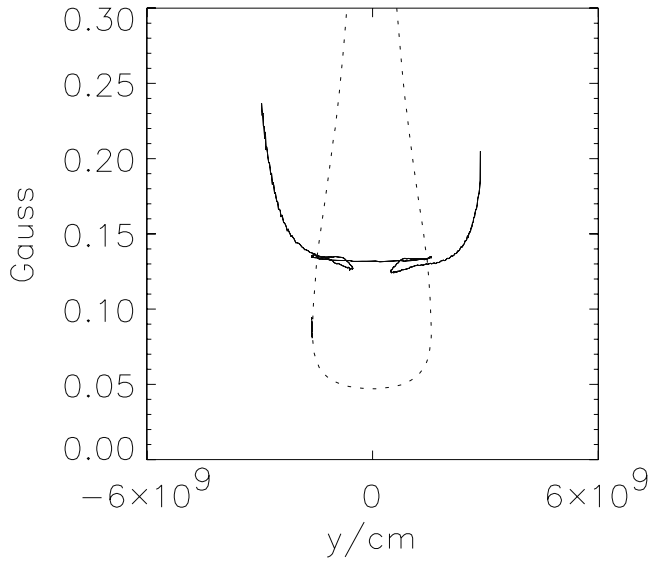

Figure 6. The magnitudes of the longitudinal and transverse field components of a coronal field line are plotted as functions of horizontal distance, y, and are shown as solid and dashed lines, respectively at time t = 8.0 hr. The field strengths apply to the same isolated coronal magnetic field line depicted in Figure 5a. The solid line clearly illustrates the development of a gradient in the longitudinal field strength that results in Lorentz forces, shearing the legs of the arcade in opposite directions.

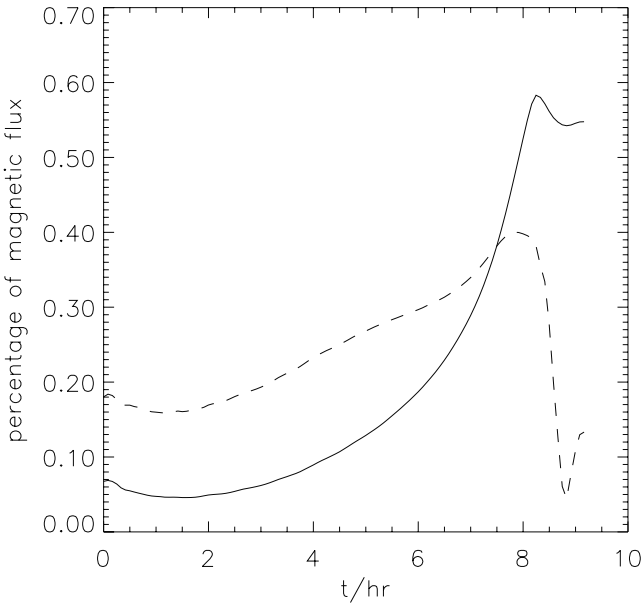

Figure 7. The percentage of longitudinal magnetic flux of the coronal system that accumulates in the expanding portion of the arcade ($z > 2.0 \times 10^9$) cm is shown as a solid line. The percentage of the transverse flux in the same expanding region is plotted as dashed line. Notice that the longitudinal flux increased by a factor of 8.5 while the transverse flux only increases by a factor of 2.0.

respectively. The resulting magnetic tension force shears the arcade with motion that can be characterized as a large-amplitude shear Alfvén wave. Examining Figure 5b clearly shows this shearing motion whose direction is consistent with the direction of the Lorentz force implied from Figure 6. By this physical mechanism, expanding motion in the plane of variation of the arcade induces a tension force to drive motion out of the plane. The shearing motions transport longitudinal flux from the legs of the arcade into the expanding loop and act to return B_x to a constant value along field lines. This effect is seen in Figure 6, where at the crest of the loop, B_x is uniform in value. At this locality, where the plasma β is low, the Alfvén speed is sufficiently high for B_x to have already equilibrated by self-induced shearing motions.

[33] During the evolution of the system, a significant amount of longitudinal flux is transported into the expanding arcade by shear Alfvén waves. To measure this effect, we integrate the longitudinal flux that has risen into the magnetic arcade above a height of $z = 2.0 \times 10^9$ cm. We also integrate the transverse flux that rises above the same height through the x-z plane centered on the rising loop. Figure 7 shows the percentages of the total longitudinal and transverse flux that rise in the atmosphere as a function of time during the growth of the instability. At $t = 8.30$ hr a maximum of 40 percent of the transverse flux of the arcade has risen above a height of 2.0×10^9 cm while 60 percent of the longitudinal flux has risen above the same height. What is significant is that while the percentage of transverse flux increases by only a factor of 2, the longitudinal flux increases by a factor of nearly 9. Thus, motion in the plane of variation can not account for the wide differences in flux transport, especially given the uniform distribution as seen in the initial state in Figure 2. Rather, Alfvén waves traveling the lengths of the field lines are essentially transporting large fractions of the longitudinal flux into the expanding portion of the arcade. When the field lines reconnect as they did in Model 1, the longitudinal flux that has accumulated in the sheared arcade is ejected into an isolated flux rope.

[34] The action of shear Alfvén waves transports longitudinal flux to the expanding portions of the magnetic field and in most circumstances, would tend to evolve B_x to constant values along the length of the field lines and restore force balance in the x direction [*Manchester and Low*, 2000]. In this case, shear Alfvén waves transport longitudinal flux from the legs to the loop crests in the arcade while also shearing footpoints of the arcade. In response, the upper portion of the arcade expands so much from the shear-induced inflation that, rather than evolving to a constant value, B_x actually grows *weaker* in the expanding portion of the arcade relative to that in the legs that are confined in dense plasma. In essence, the pressure gradient over the height of the expanding arcade, leads to a gradient in Bx that results in a Lorentz force that shears the arcade. The increasing gradient in B_x promotes more shearing and greater inflation of the arcade. The resulting positive feedback between arcade expansion and self-induced shearing leads directly to a catastrophic loss of equilibrium and the eruption of the arcade. As the arcade erupts, the expanding field lines continue to shear and accumulate flux until the field lines are cut by reconnection. A previous analytical study of a magnetic arcade with an embedded filament determined the system to be susceptible to loss of equilibrium [*Forbes and Isenberg*, 1991]. In this case, no equilibrium states were possible when magnetic foot-points were brought together by a convergent flow. Here, the loss of equilibrium occurs when the condition for force balance in the x direction, namely that B_x be constant along field lines, becomes incompatible with pressure balance in the z direction as the arcade expands in the gravitationally stratified atmosphere.

3.3. Energetics of the Eruption

[35] Since the system is undriven and the energy released in the arcade eruption is more than 1000 times greater than that imparted by the velocity perturbation, the energy must naturally come from the pre-event coronal initial state. To determine the energy source, we plot the change in magnetic, gravitational and thermal energies of the system relative to the initial state in Figure 8. Since our system possesses uniform gravity, we calculate the gravitational binding energy with respect to an arbitrarily chosen reference height rather than integrating from infinity. In this case, the sign and magnitude of the gravitational energy are arbitrary, while the relative change in energy remains physically meaningful.

[36] Examining the plots of the change in total energies in the top panel, we are immediately struck by the fact that the magnetic energy increases prior to and during the eruption by a total amount of 1.41×10^{17} ergs cm^{-1} and then decreases only with the onset of magnetic reconnection. By comparison, the gravitational and thermal energies decrease by 2.56×10^{17} and 7.70×10^{16} ergs cm^{-1} respectively,

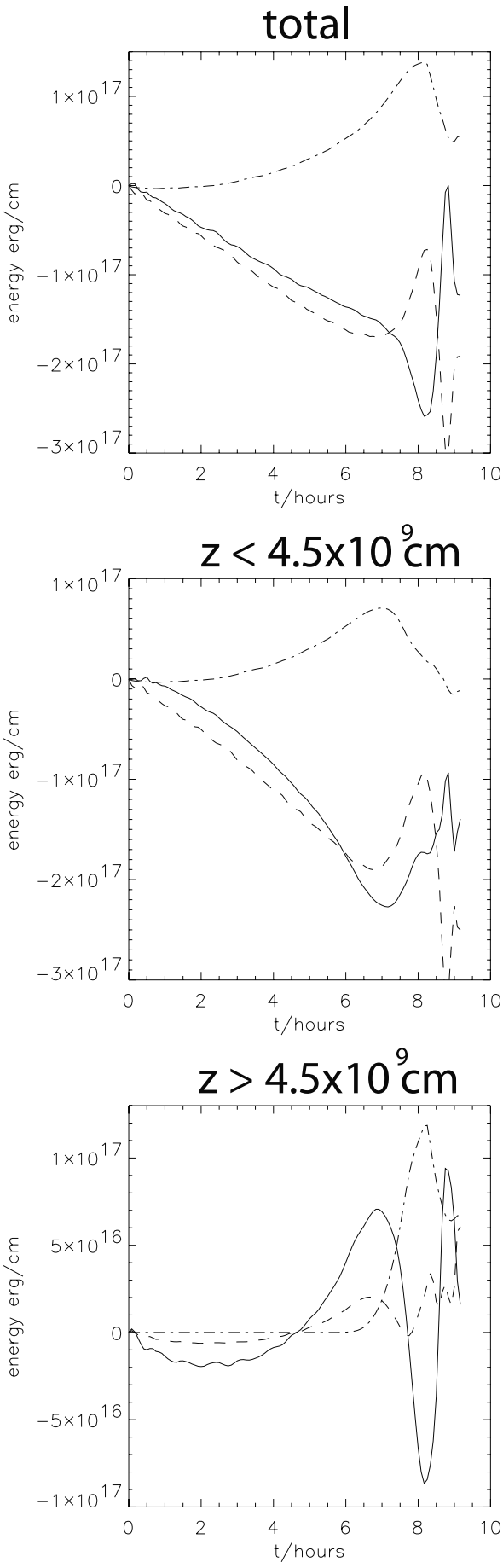

more than enough to account for the increase in magnetic energy and kinetic energy (5.0×10^{16} ergs cm^{-1}). The changes in energy are rather modest compared to the total magnetic (7×10^{17} ergs) and thermal energy (2×10^{19} ergs) of the initial state but still drives a substantial eruption in the stratified atmosphere. Thermal energy dominates since the magnetic field fills only a small percentage of the total volume. There is a loss of 0.75 percent of the total energy but approximately 30 percent of the drop in gravitational and thermal energy. This small decrease in total energy we believe is due to numerical dissipation.

[37] During the short-lived eruption, kinetic, magnetic and thermal energies all increase and only gravitational energy decreases. From this analysis, we conclude that energy for the eruption comes from magnetic buoyancy. In this case, there are aspects of the eruption that are inconsistent with the magnetic loop being passively drawn upwards by the gravitational stratification of the surrounding atmosphere. First, the plasma β of the rising loop lies between 10^{-2} and 10^{-4} before and during the eruption respectively. Consequently, magnetic pressure and energy exceeds that of the surrounding atmosphere. Second, as seen in Figure 4, the rise velocity of the loop reaches values of 140 km s^{-1}, whereas the ambient sound speed is 80 km s^{-1}, which is also consistent with a magnetic pressure driving the expansion of the upper portion of the arcade. The increase in magnetic energy during the eruption shows the instability to be buoyant in nature with gravitational and thermal pressure ultimately driving the evolution.

[38] To understand the energetics of the eruption, we need to determine where the energy is changing. We accomplish this by plotting energies for $z < 4.5 \times 10^9$ cm in the center panel, and in the right panel, we plot energies in the region $z > 4.5 \times 10^9$ cm. This separation of the computed energies occurs at a location that is only 10 percent of the distance from the bottom to top of the domain. This location is chosen because this is where magnetic reconnection sets in and marks the point of separation between the erupting magnetic field and the reformed arcade. Examining the magnetic energy plots for the two spatial regimes, we find that the magnetic energy in the lower arcade increases until the time of the eruption. Then, as the arcade erupts, magnetic energy increases above $z = 4.5 \times 10^9$ cm as the field expands beyond this height and simultaneously the magnetic energy below this line decreases below the initial value.

Figure 8. (opposite) The change in magnetic, gravitational and thermal energies from the coronal system are shown in Figure 6 as dot-dash, solid and dashed lines respectively. The top panel shows the energies integrated over the entire domain, the center panels shows energies integrated over the domain $z < 4.5 \times 10^9$ cm and the bottom panel shows energies for the domain $z > 4.5 \times 10^9$ cm. The figures depict a marked difference in the time evolution of energies of the erupting portion of the arcade ($z > 4.5 \times 10^9$ cm) and the region in which the field lines remain nearly settled ($z < 4.5 \times 10^9$ cm). Also notice the general trend that gravitational and thermal potential energies are transferred to magnetic energy, which is then dissipated at the onset of magnetic reconnection.

[39] At first, it appears as though magnetic energy has simply been advected from one region to the other. However, upon examining the velocity profiles in Figure 4, we find that the vertical velocity remains near zero below $z = 4.5 \times 10^9$ cm hours before the eruption. Hence, the magnetic field is not advected beyond this point, but rather is being vertically stretched. This can be easily seen in the field lines of the arcade below $z = 4.5 \times 10^9$ cm, which remain nearly stationary throughout the eruption. If motions were confined to the plane of variation, we could understand the magnetic energy above the upper arcade increasing from the stretching distortion; however, these motions do not explain the decrease in magnetic energy below this point. In fact, the total magnetic energy remains nearly constant during the rapid increase (decrease) of magnetic energy above (below) the stagnation point, so clearly, magnetic energy has been transferred from the lower to the upper arcade.

[40] The explanation for the energy transport comes from the fact that motions are not confined to the plane of variation. Rather, the self-induced shearing motions in the x direction transport longitudinal magnetic flux (see Figure 7) and its associated energy to the expanding portion of the arcade. While shear Alfvén waves are the energy transport mechanism, we find the ultimate source of energy necessary for the eruption is gravitational energy released below the height of reconnection in the high β portion of the arcade. Liberated gravitational energy goes largely into magnetic energy and the magnetic energy appears in the upper portion of the expanded sheared arcade. By comparison, the maximum drop in gravitational energy of the upper atmosphere is less than half that required to account for the increase in magnetic and kinetic energy in the same region of space. Furthermore, we find that by the end of the eruption, both the thermal and gravitational energies of the upper atmosphere are higher than their original values while the magnetic, thermal and gravitational energies below the reconnection point are lower than found in the initial state.

[41] As mentioned earlier, the arcade eruption results from a feedback between arcade expansion and self-induced shearing. However, the analysis of the energetics demonstrates more clearly the significance of plasma pressure and weight in the gravitationally stratified atmosphere. The force-balance condition in the invariant direction requires the B_x to be constant along the entire length of a field line. As the arcade evolves, shear Alfvén waves transport longitudinal flux from the bottom to the top of the arcade over many pressure scale-heights. The Alfvén waves redistribute the longitudinal flux and its associated energy from the from the high-β plasma-confined legs of the arcade to the upper arcade, which by comparison, is expanding into a near-vacuum. The dense atmosphere moves downward as it compresses the legs of the arcade which sustains the gradient in B_x which in turn sustains and ultimately drives the shearing motion along the entire length of the field line. The stratification of the atmosphere is essential for the arcade to erupt. Not only is the energy derived from the high-β portion of the arcade, but the pressure of the atmosphere falls off sufficiently with height that the arcade expands out of equilibrium from shear-induced inflation. In this way, the demand for B_x to be constant along the length of field lines and the condition of pressure balance become incompatible for equilibrium as the arcade expands and passes vertically over several pressure scale-heights.

3.4. Model 2 Results

[42] For Model 1, we chose a relatively weak initial magnetic field resulting in a plasma β higher than one might typically expect to find in the corona. The plasma beta of the initial state is significant to the simulation in the following sense. The most important features of the initial state in driving the instability is a sheared structure embedded in a highly pressure stratified background atmosphere. The instability would not occur if the lower extremity of the arcade were not in a plasma pressure dominated regime. It is the pressure gradient that sustains the gradient in B_x that drives the shearing motion. However, the upper part of the arcade need not be of a high plasma β and in fact, we find that the expanding portion of the arcade proceeds to a very low β during the onset of the instability. Clearly, magnetic arcades in the Sun do pass through a highly stratified plasma reaching a high beta state below the chromosphere. Clearly, simulations with more realistic initial states are needed to expand upon the basic results presented here. To give an idea of how this buoyancy instability is dependent upon physical conditions of the arcade, we present a second simulation. For model 2, the atmosphere is chosen to have a photospheric temperature and a plasma β twice as high as model 1. Also, the arcade is prescribed with a flux function $A(\phi)$, that more evenly distributes the magnetic field over the height of the arcade. The general purpose of this model is to test how the results of the arcade instability found in model 1 will apply to a different arcade in a different solar regime.

[43] To begin the simulation, the photospheric arcade of model 2 is given a velocity perturbation prescribed by equation (25) with the amplitude scaled down relative to the lower sound speed of the system. We find in Figure 10 that the system responds to this perturbation with a very modest and irregular growth in kinetic energy that roughly increases with an e-folding time of 28τ (0.18 hr). The energy increases in this way for the first 0.28 hours during which time the arcade gradually expands upwards and spontaneously shears as can be seen as purple regions in Figure 9. In this case, the shear velocity is much less than that of model 1, with footpoints moving at speeds less than 1 km s^{-1}. At $t = 0.33$ hr, the system enters a period of super-exponential growth in kinetic energy, which corresponds to the rapid rise of the upper portion of the arcade, as seen in the lower left frame of Figure 9. The kinetic energy reaches a maximum value at approximately $t = 0.45$ hr, corresponding with the ejection of a flux rope that has formed by the pinching off and reconnection of the arcade field lines. In this case, flux rope moves slowly off the upper boundary as can bee seen in Figure 9. When the flux rope is cut at the boundary, the field lines unshear resulting in its red and black color.

[44] After this eruption, the arcade settles down and one would believe that the system, having expended its free energy, would now approach an equilibrium state. However, what is truly remarkable about this simulation is that the evolutionary sequence of a slow rise culminating in the eruption of the magnetic arcade is found to repeat. After the

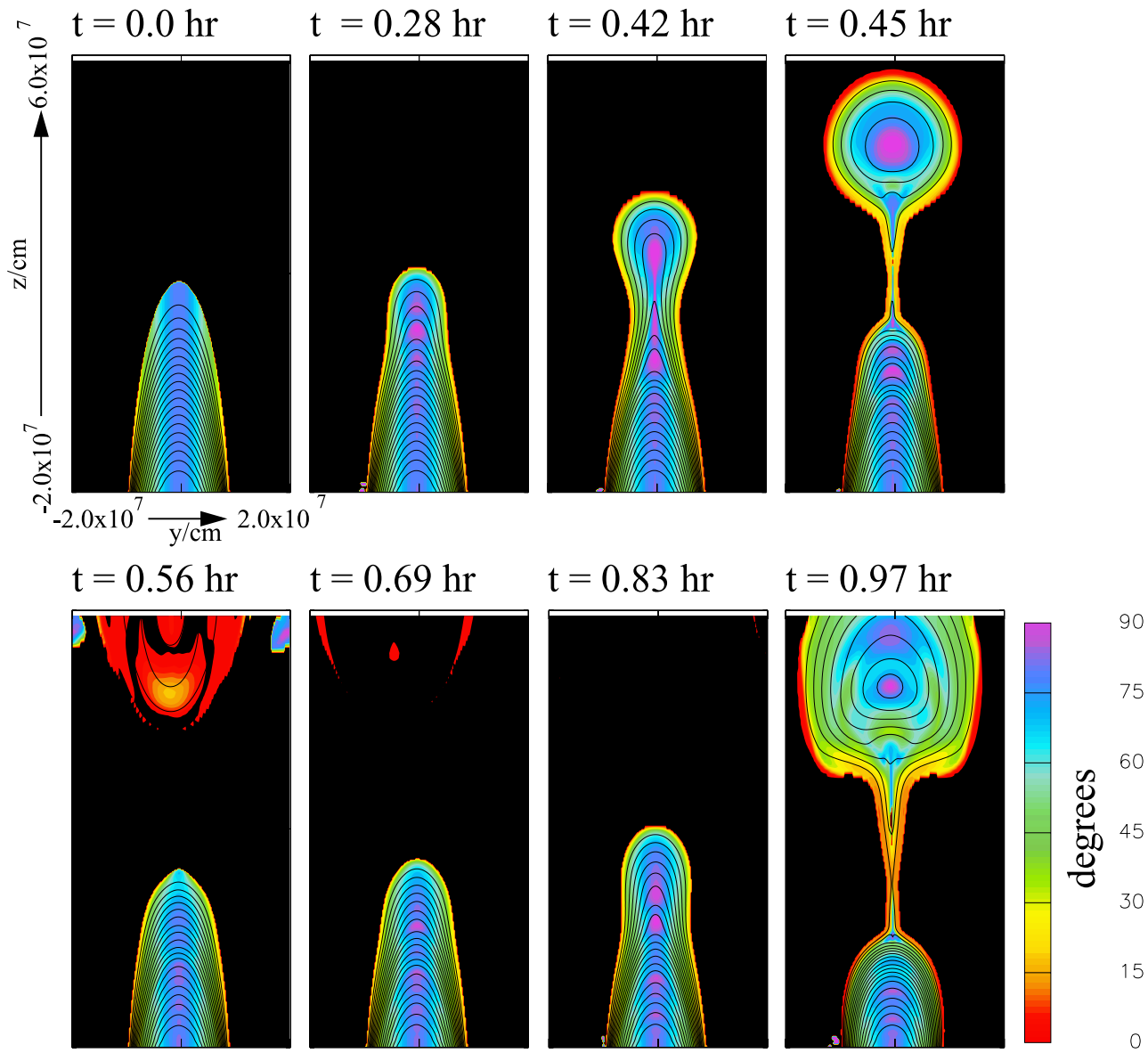

Figure 9. Results for the photospheric model. Depicted is a time sequence of images showing the evolution of the magnetic field of the coronal arcade for times t = 0.0, 0.28, 0.42, 0.45, 0.56, 0.69, 0.83, and 0.97 hr. The magnetic field is displayed as field lines projected on the y-z plane in black and the shear angle measured between the field lines and the plane of variation is shown in false color. The evolution occurs slowly as the field lines in the upper part of the arcade begin to expand upwards and spontaneously shear. At time t = 0.45 hr, we see that the arcade erupts upwards and necks off in the process. Magnetic reconnection occurs and a flux rope is ejected from the arcade. Afterward the arcade continues to expand after the eruption however, we now find that the location of increased magnetic shear occurs further down in the arcade. In the final frame of the series, we see that the arcade erupts a second time to produce a flux rope that is larger and contains twice as many field lines as the first ejected flux rope.

first eruption, longitudinal flux continues to accumulate on expanding portions of field lines. These field lines are in the midsection of the arcade and were not involved in the first eruption. When the second eruption occurs (see Figure 9), it involves twice as many field lines as the first. The difference can be clearly seen in the first and second flux ropes ejected from the arcade, which contain four and eight field lines respectively. Consistent with the difference in field lines, inspection of Figure 10 reveals that the second eruption is 2.7 times more energetic than the first. With successive eruptions, the arcade relaxes to a less sheared state.

4. Comparison With Observations

[45] Observations of the solar corona with Yohkoh have revealed X-ray plasma ejections from cusp-shaped loop structures associated with long duration event (LDE) flares

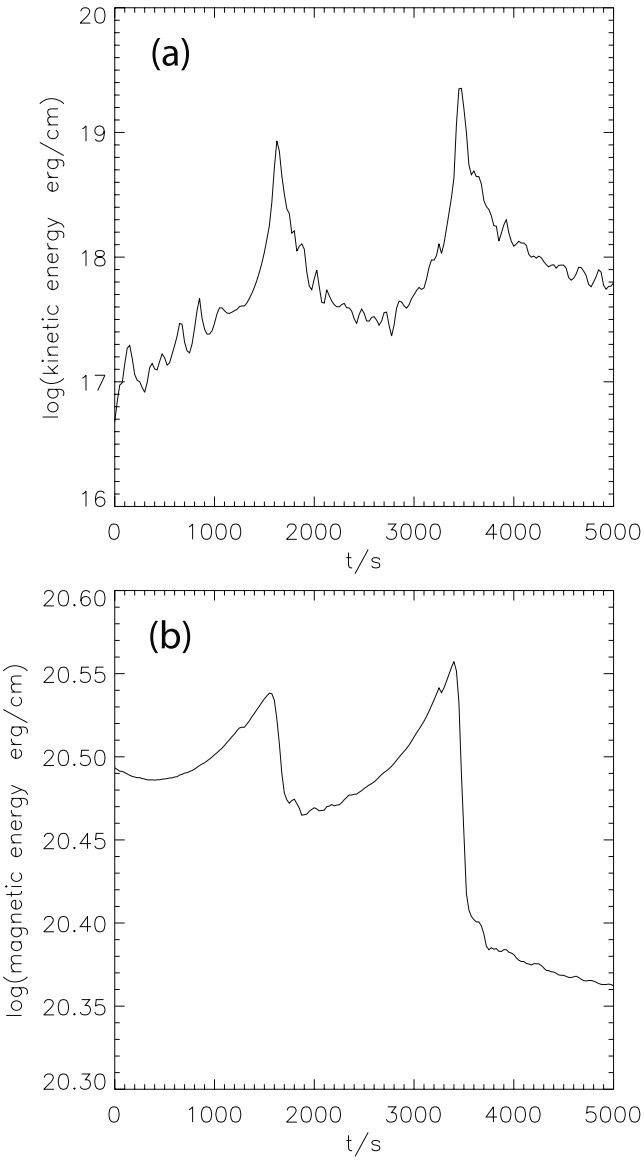

Figure 10. The magnetic and kinetic energy of the photospheric system are shown as functions of time in Figures 10a and 10b, respectively. During the first 1000 s after the system is perturbed, the kinetic energy increases very little as the arcade slowly expands. Between 1200 and 1600 s, the kinetic energy enters a period of super-exponential growth as the arcade erupts, culminating in the ejection of a flux rope at 1625 s. Afterward, the kinetic energy drops to a nearly constant level as the arcade evolves nearly quasi-statically. At 3000 s the kinetic energy again enters a phase of super-exponential growth associated with the arcade's second eruption. The magnetic energy increases simultaneously with the kinetic energy and then drops at the onset of magnetic reconnection.

as well as plasma emitted from compact impulsive flares. The plasmoid ejection from loops can be described as a sequence of events in which the upper portion of an arcade rises up, necks off, and separates as a isolated plasmoid moving upwards. A survey by *Shibata et al.* [1995] found that such events occurred within the range of velocities of 50–400 km s^{-1}, a range of sizes, (4–10) $\times$ 10^9 cm, and kinetic energies in the range 10^{27}–10^{28} ergs. Plasmoid ejection can be interpreted by the physical model in which the magnetic field of an arcade stretches upwards, pinches together to form a current sheet and magnetically reconnects above the arcade. An example of a recent numerical simulation of this process is given by *Magara et al.* [1997]. Here, we find similar behavior in our numerical model. In comparison, the simulated eruption in Figure 2 has a similar appearance to a plasmoid ejection from a flare loop [*Ohyama and Shibata*, 1998] as well as possessing physical properties that are consistent with observations [*Shibata et al.*, 1995]. In our model, the arcade measures 8.0×10^9 cm at the base. The flux rope is ejected with a velocity of 140 km s^{-1} and a kinetic energy of 6.0×10^{26} ergs (assuming the arcade extends no farther in the invariant direction than it does in the y direction).

[46] This model of arcade eruption may have implications to CMEs which are characterized by being 3–4 orders of magnitude more energetic than plasmoid ejections, and 10–100 times larger in spatial dimensions. The simulated coronal arcade eruption is too small to represent a typical CME fully. However, if the arcade is scaled to the size and field strengths of a typical helmet streamer, the eruption may yield the necessary 10^{31} ergs of kinetic energy for a CME. The question remains whether the shearing motions driven by the Lorentz force as suggested can deliver sufficient power to drive a CME. While high pressure is required near the base of the arcade to sustain the shearing, high density will slow down the shearing motion to a characteristic fraction of the Alfvén speed. It is more likely that such a mechanism could apply to slow CMEs for which energy is delivered over a long period of time compared to fast CMEs. Also, it is possible that such shearing could provide a build up of energy and magnetic flux over a long period of time while some other mechanism allows that energy to be released quickly in a CME. Finally, this model predicts that the legs of an arcade should compress as well as shear at the photosphere during an eruption. Observational examples of shear flows are common, while it is not clear that such a compressive flow is present.

[47] In spite of these limitations, the model eruption does possess features associated with CMEs. First, the pre-event structure of our model, a sheared arcade possessing a cavity is consistent with the facts that all CMEs originate from coronal structures overlying sheared photospheric neutral lines and that a common precursor of CMEs is the presence of a low-density cavity located above the neutral line. Hours before the eruption the coronal arcade swells and develops a highly sheared core where the field lines are expanding. These behaviors are consistent with observations that many CMEs begin with a slow swelling of coronal streamers on a time-scale of 4–5 days [*Hundhausen*, 1993] and the magnetic field of pre-event arcades is greatly sheared, running parallel to the neutral line [*Falconer*, 2001]. In conjunction with high shear, arcades observed in X-ray are found to develop a prominent sheared core that takes the form of a sigmoid tracing the neutral line [*Moore et al.*, 2001].

[48] In our simulation, magnetic shear of the arcade field lines is greatly reduced during magnetic reconnection that produces an isolated flux rope. While shear reduction with

reconnection has long been recognized [*Pneuman*, 1983], here loss of shear is far more significant, given the accumulation of longitudinal flux by Alfvén wave in the expanding magnetic loop that becomes the flux rope (see Figure 5a). A loss of magnetic shear from reconnection associated with CMEs is observed in conjunction with two-ribbon flares. These flares occur after CMEs lift off and are interpreted as the result of reconnection of coronal magnetic fields opened up by an outgoing CME [*Low*, 1996]. Concurrent with two-ribbon flares is a significant reduction of magnetic shear observed in Hα arches [*Zirin and Tanaka*, 1981; *Zirin*, 1984]. A loss of shear after CMEs is also observed with the transformation of sigmoids to potential-like X-ray arcades possessing loops almost perpendicular to the neutral line [*Sterling and Hudson*, 1997; *Moore et al.*, 2001]. Finally, we note that the outgoing flux rope of our model is consistent with the identification of interplanetary magnetic clouds as CMEs in the solar wind as observed by *Burlaga et al.* [1998].

4.1. Homologous Eruptions

[49] The dynamics exhibited by the photospheric arcade may have implications for activity and flaring observed at bipolar active regions. The free energy stored in sheared magnetic fields has long been considered the primary source of energy released in flares. Consistent with this belief are observations that flares most often occur along the most sheared portions of magnetic neutral lines. Furthermore, we find that as magnetic shear is lost from the upper portion of the arcade to the ejected flux rope, magnetic shear continues to increase deeper down in the arcade. This natural tendency of the magnetic field to remain sheared after reconnection is consistent with evidence of fields that remain persistently sheared throughout a period of flaring as observed by *Hagyard et al.* [1984]. Finally, it is often observed that flares are homologous in the sense that they reappear at the same location with comparable energy, a characteristic clearly seen in the multiple eruptions of the photospheric arcade. In our photospheric model, we find there is sufficient energy in the magnetostatic structure for multiple eruptions, which is consistent with observations of homologous flares.

4.2. Shear Velocity

[50] Our models of arcade eruptions offer many comparisons and interpretations of observations of expanding magnetic loops in the solar corona. In particular, the mode of instability by which the arcades erupt involve strong shearing motions. Recent observations at the solar limb by the Solar Ultraviolet Measurements of Emitted Radiation (SUMER) on board the Solar and Heliospheric Observatory (SOHO) have revealed significant velocity shear in active region loops expanding high into the transition region [*Chae et al.*, 2000]. Of particular significance are loops expanding at velocities estimated at 25 km s^{-1} whose line-of-sight velocity exhibits a velocity shear of 50 km s^{-1}. The velocity changes sign at the axis of the loop leading the authors to interpret the velocity as bulk rotational motions. Based on our simulations, we suggest the velocity shear can be attributed to shear Alfvén waves which we suggest is consistent with the expansion of the loops. Furthermore, for CMEs and plasmoid ejections observed above the disk, we predict line-of-sight shear velocities to have magnitudes of 100 km s^{-1} or greater. This mechanism for velocity shear is consistent with *Manchester* [2001] that explains observed shearing motions at the photosphere [*Strous et al.*, 1996], chromosphere [*Malherbe et al.*, 1983] and transition region [*Athay et al.*, 1985] in terms of Alfvén waves generated during flux emergence.

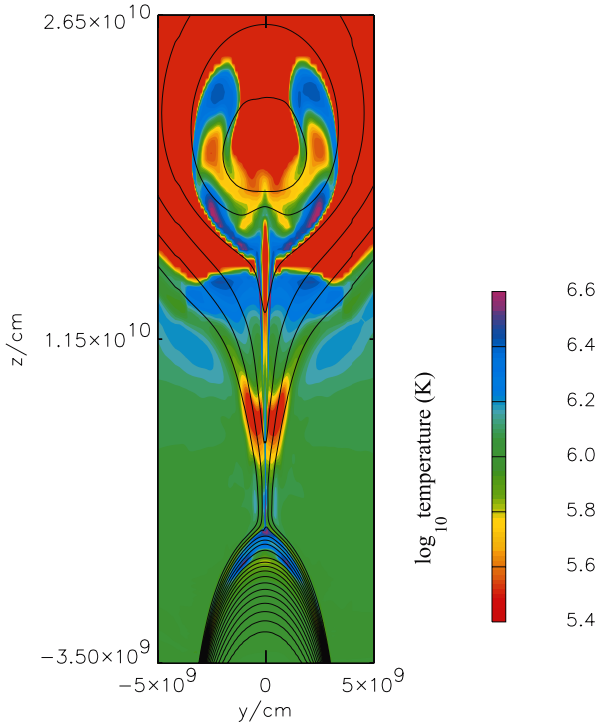

Figure 11. Magnetic field lines shown in black are superposed on a false color image of the plasma temperature at t = 8.30 hr. The forming flux rope has cooled from adiabatic expansion except for two distinct regions heated by MHD shocks. At the base of the forming flux rope, a shock has formed from plasma falling down the expanding arcade. A second shock, driven by the reconnection jet, engulfs the center of the flux rope. In both cases, plasma is heated to more than 3×10^6 K.

4.3. Density and Temperature

[51] A discussion of our work would be incomplete without mentioning the densities and temperature predicted by our model. Here, the arcades erupt as an ideal MHD process only after which magnetic reconnection occurs and produces high speed jets. These jets produce localized heating of the plasma, with an MHD shock at the base, and around the core, of the forming flux rope whereas most of the volume of the flux rope is cooled by adiabatic expansion (Figure 11). We also find heating at the cusp of the re-forming arcade that is similar to hot cusps found on post-CME arcades observed in soft X-rays by *Moore et al.* [2001]. The heating we attain in our model is due to adiabatic compression and shock heating while Joule heating has been neglected. This result is certainly significant, given that the magnetic energy lost through numerical diffusion is twice as great as the kinetic energy of the eruption.

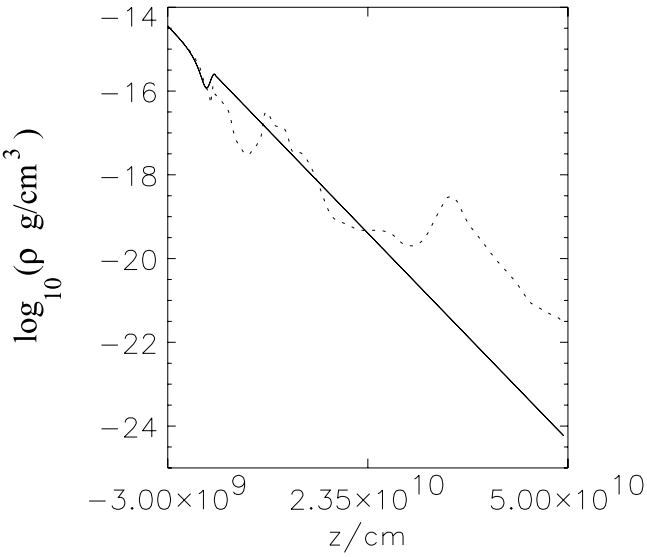

Figure 12. Plasma density for the coronal model is plotted at a function of height (z) through the center of the system at times $t = 0.0$ (solid line) and $t = 8.30$ hr (dashed line). The solid line clearly shows the density depleted cavity of the initial state and the exponential drop-off of density in the isothermal atmosphere. At the later time, the dashed line shows a large pileup of plasma in front of the erupting arcade and density enhancements (relative to the background atmosphere) in the bottom of the forming flux rope. A modest depletion of density is visible near the top of the expanding magnetic field.

[52] Finally, in Figure 12 we plot the density as a function of height in the center of the system at 8.30 hr. Here we find a pile-up of plasma ahead of the arcade that is nearly 100 times denser than the ambient atmosphere. In the forming flux rope, there are modest density depletions and enhancements at the top and bottom respectively. The density structure only qualitatively represents the three-part structure of CMEs observed in coronagraphs. The discrepancies are largely due to the absence of both erupting prominence material and solar wind in our model.

5. Discussion and Conclusions

[53] It has become a paradigm of solar physics that magnetic fields evolve to sheared configurations as a result of footpoint displacements that are driven by photospheric flows. Numerous physical models prescribe such footpoint motion of coronal magnetic arcades to provide a buildup of magnetic shear that ultimately leads to the disruption of arcades as shown by *Mikić et al.* [1988], *Choe and Lee* [1996], *Mikić and Linker* [1994], and *Wolfson* [1995]. We offer an alternative view for the initiation of slow CMEs, namely that they are the result of an undriven magnetic buoyancy instability. The particular mode of instability couples buoyancy, self-induced shearing, and shear-induced inflation that leads arcades to a loss of equilibrium and eruption. In this case, energy for the eruption exists in the pre-event non-force-free equilibrium configuration in which the lower part of the magnetic arcade is embedded in and compressed by high β plasma. An attractive quality of the instability is that it develops over a long period of time, during which the arcade expands from self-induced shearing. This behavior lends itself as an explanation for the observation of helmet streamers swelling days before they erupt in CMEs. Most importantly, we find that the shearing motions are driven by the Lorentz force, and take the form of nonlinear Alfvén waves acting to transport longitudinal flux to the expanded portion of the magnetic arcade. The irrepressible tendency for the magnetic shear to propagate as Alfvén waves into the expanding arcade, is the Cartesian version of the propagation of twist into the expanding part of an emergent magnetic flux rope by torsional Alfvén waves as suggested by *Parker* [1979].

[54] The transport of magnetic flux is particularly significant when viewed in the context of recent simulations by *Manchester* [2001] and *Fan* [2001], which show that shear Alfvén waves generated during flux emergence bring magnetic shear from deep below the photosphere into magnetic arcades rising into the corona. Unlike past models, shear is not being generated by imposed photospheric flows, rather it is transported from extensive magnetic structures below the surface. In our simulations, we find that such accumulated shear is lost from the system when the arcade erupts to eject a flux rope. The transport properties of shear Alfvén waves in the formation of arcades during flux emergence, and the subsequent eruption of arcades in CMEs, suggest that CMEs play a significant role in the long term evolution of the solar magnetic field. Specifically, magnetic shear (toroidal flux) created on a global scale by differential rotation accumulates in the buoyantly rising magnetic field by the action of shear Alfvén waves, and is removed from the sun by CMEs.

[55] A connection between CMEs and the global magnetic field has been strongly suggested from recent observations. First, *Hundhausen* [1993] has shown that the distribution of CMEs is closely related to large-scale magnetic structures such as prominences and that CMEs even follow the tilt of the magnetic dipole near solar minimum. In this same study it was found that as the solar cycle progresses, the majority of CMEs originate from helmet streamers at higher and higher latitudes even as magnetic flux is found to emerge at progressively lower latitudes. These high latitude CMEs are associated with large quiescent prominences that also seem linked to the global magnetic field. First, the axial field of such polar crown filaments is inconsistent with a field that would be created by differential rotation acting on a line-tied preexisting coronal magnetic field [*Rust*, 1967]. However, it has been pointed out by *Van Ballegooijen and Martens* [1990] that the axial field of these filaments can be created by differential rotation below the photosphere. Finally, it has been observed that the rotation rates of these pre-event structures deviate significantly from the photosphere, which may be taken to imply that the fields are rooted deep below the photosphere as suggested by *Mouradian et al.* [1987].

[56] While there is a clear case for CMEs originating from the loss of equilibrium from large-scale helmet streamers, some CMEs have also been shown by *Feynman and Martin* [1995] to be correlated to emerging flux in active regions. Furthermore, these active region CMEs tend to be of a high-speed ballistic nature in contrast to the more gentle acceleration of CMEs from long-lived helmet streamers [*Sheeley et al.*, 1999]. The difference in speeds has lead *Gosling et al.*

[1976] to suggest that there are two distinct classes of CME, fast and slow. It is possible that an arcade eruption, in the context of our simulations, provides a mechanism for driving slow CMEs from a pre-event, streamer in which the magnetic field lines deeply penetrate the solar interior. In this case, the accumulation of toroidal flux by shear Alfvén waves takes a long period of time, and leads to gradual loss of equilibrium leading to slow ejection of plasma (<800 km/s). In contrast, active region CMEs originate from strong-field near-surface fields that erupt at velocities difficult to account for with a buoyancy related mechanism.

[57] There are simplifying assumptions in our model for arcade eruption that should be remarked upon. First, the 2.5D simulations presented here take the arcades to be infinitely long. For a realistic 3D arcade that is finite in length, self-induced shearing motion would likely diminish near the ends of the arcade. Another limitation is the isothermal nature of our initial states which prevents us from modeling arcades passing through a temperature-stratified model atmosphere. Finally, the uniform gravity and Cartesian geometry of our system restricts our model arcades to sizes that are small compared to helmet streamers that typically extend to 2–3 solar radii. In spite of these limitations, we believe that the physical processes found to guide the evolution of our 2D symmetric arcades are a significant step toward understanding the much more complex and realistic 3D configurations.

[58] **Acknowledgments.** I thank B.C. Low, Dimitri Mihalas, Paul Charboneau, Tom Holzer and Tamas Gombosi for discussion and comments concerning the manuscript. I am indebted to Jim Stone and Mike Norman for consultation regarding the use and understanding of the ZEUS-2D code. The simulations reported here were carried out on an Origin 2000 supercomputer at NCSA. While performing the research for the manuscript, I was supported by a Gordon Newkirk Graduate Assistantship and a NASA grant at the High Altitude Observatory. The National Center for Atmospheric Research is sponsored by the National Science Foundation. During this time, I was also supported in part by the McVittie Professor Fund of the University of Illinois. The manuscript was prepared for publication while I was supported by DOD grant F49620-01-1-0359 and NFS grant ATM-9980078 at the University of Michigan.

[59] Shadia Rifai Habbal thanks Kazunari Shibata and Terry G. Forbes for their assistance in evaluating this paper.

References

Aly, J. J., How much energy can be stored in a three-dimensional force-free magnetic field?, *Astrophys. J. Lett.*, *375*, L61–L64, 1991.

Antiochos, S. K., C. R. DeVore, and J. A. Klimchuk, A model for solar coronal mass ejections, *Astrophys. J.*, *510*, 485–493, 1999.

Athay, R. G., H. P. Jones, and H. Zirin, Magnetic shear, I, Hale region 16918, *Astrophys. J.*, *288*, 363–372, 1985.

Burlaga, L. F., et al., A magnetic cloud containing prominence material: January 1997, *J. Geophys. Res.*, *103*, 277–286, 1998.

Chae, J. C., H. Wang, J. Qiu, and P. R. Goode, Active region loops observed with SUMER on board the Solar and Heliospheric Observatory, *Astrophys. J.*, *533*, 535–545, 2000.

Chen, P. F., and K. Shibata, An emerging flux trigger mechanism for coronal mass ejections, *Astrophys. J.*, *545*, 524–531, 2000.

Choe, G. S., and L. C. Lee, Evolution of solar magnetic arcades. II. Effects of resistivity and solar eruptive processes, *Astrophys. J.*, *472*, 372–388, 1996.

Dryer, M., S. Wu, R. S. Steinolfson, and R. M. Wilson, , *Astrophys. J*, *227*, 1059, 1979.

Falconer, D. A., A prospective method for predicting coronal mass ejections from vector magnetograms, *J. Geophys. Res.*, *107*(A11), 25,185–25,190, 2001.

Fan, Y., The emergence of a twisted Ω-tube into the solar astmosphere, *Astrophys. J. Lett.*, *554*, L111–L114, 2001.

Feynman, J., and S. F. Martin, The initiation of coronal mass ejections by newly emerging magnetic flux, *J. Geophys. Res.*, *100*, 3355–3367, 1995.

Forbes, T. G., and P. A. Isenberg, A catastrophe mechanism for coronal mass ejections, *Astrophys. J.*, *373*, 294–307, 1991.

Forbes, T. G., and E. R. Priest, Photospheric magnetic field evolution and eruptive flares, *Astrophys. J.*, *446*, 377–389, 1995.

Gibson, S., and B. C. Low, A time-dependent three-dimensional magneto-hydrodynamic model of the coronal mass ejction, *Astrophys. J.*, *493*, 460–473, 1998.

Gosling, J. T., E. Hildner, R. M. MacQueen, R. H. Munro, A. I. Poland, and C. L. Ross, The speeds of coronal mass ejection events, *Sol. Phys.*, *48*, 389–397, 1976.

Hagyard, M. J., R. L. Moore, and A. G. Emslie, The role of magnetic field shear in solar flares, *Adv. Space Res.*, *4*, 71–80, 1984.

Howard, R. A., et al., Observations of CMEs from SOHO/LASCO, in *Coronal Mass Ejections, Geophys. Monogr. Ser.*, vol. 99, edited by N. Crooker, J. A. Joselyn, and J. Feynman, pp. 17–26, AGU, Washington, D.C., 1997.

Hundhausen, A. J., The origin and propagation of coronal mass ejections, in *Proceedings of the Sixth International Solar Wind Conference, NCAR TN-306*, edited by V. J. Pizzo, T. E. Holzer, and D. G. Sime, pp. 181–214, Natl. Cent. for Atmos. Res., Boulder, Colo., 1987.

Hundhausen, A. J., Sizes and locations of coronal mass ejections: SMM observations from 1980 and 1984–1989, *J. Geophys Res.*, *98*, 13,177–13,200, 1993.

Hundhausen, A. J., Coronal mass ejections: A summary of SMM observations from 1980 and 1984–1989, in *The Many Faces of the Sun*, edited by K. Strong, J. Saba, and B. Haisch, pp. 143–200, Springer-Verlag, New York, 1999.

Kusano, K., and K. Nishikawa, Bifurcation and stability of coronal magnetic arcades in a linear force-free field, *Astrophys. J.*, *461*, 415–423, 1996.

Lin, J., and T. G. Forbes, Effects of reconnection on the coronal mass ejection process, *J. Geophys. Res.*, *105*, 2375–2392, 2000.

Linker, J. A., and Z. Mikic, Disruption of a helmet streamer by photospheric shear, *Astrophys. J. Lett.*, *438*, L45–L48, 1995.

Low, B. C., Expulsion of magnetized plasmas from coronae, in *Solar and Stellar Magnetic Fields: Origins and Coronal Effects, Proceedings of the Symposium, Zurich, Switzerland, August 2–6, 1982*, edited by J. O. Stenflow, pp. 467–471, D. Reidel, Norwell, Mass., 1983.

Low, B. C., Magnetohydrodynamic processes in the solar corona: Flares, coronal mass ejections, and magnetic helicity, *Phys. Plasmas*, *1*, 1684–1690, 1994.

Low, B. C., Solar activity and the corona, *Sol. Phys.*, *167*, 217–265, 1996.

Low, B. C., and A. J. Hundhausen, The velocity field of a coronal mass ejection: The event of September 1, 1980, *J. Geophys. Res.*, *92*, 2221, 1987.

Low, B. C., and J. R. Hundhausen, Magnetostatic structures of the solar corona, II, The magnetic topology of quiescent prominences, *Astrophys. J.*, *443*, 818–836, 1995.

Low, B. C., and W. Manchester IV, Equilibrium and stability of magnetostatic atmospheres, I, Dungey-type isothermal states, *Astrophys. J.*, *528*, 1026–1033, 2000.

Magara, T., K. Shibata, and T. Yokoyama, Evolution of eruptive flares, I, Plasmoid dynamics in eruptive flares, *Astrophys. J.*, *487*, 437–446, 1997.

Malherbe, J. M., B. Schmieder, E. Ribes, and P. Mein, Dynamics of solar filments, *Astron. Astrophys.*, *119*, 197–206, 1983.

Manchester, W., IV, The role of nonlinear Alfvén waves in shear formation during solar magnetic flux emergence, *Astrophys. J.*, *547*, 503–519, 2001.

Manchester, W., IV, and B. C. Low, Magnetostatic atmospheres possessing identical invariants of ideal magnetohydrodynamics, *Phys. Plasmas*, *7*, 1263–1279, 2000.

Mikić, Z., and J. A. Linker, Disruption of coronal magnetic field arcades, *Astrophys. J.*, *430*, 898–912, 1994.

Mikić, Z., D. C. Barnes, and D. D. Schnack, Dynamical evolution of a solar coronal magnetic field arcade, *Astrophys. J.*, *328*, 830–847, 1988.

Moore, R. L., A. C. Sterling, H. S. Hudson, and R. J. Lemen, Onset of the magnetic explosions in solar flares and coronal mass ejections, *Astrophys. J.*, *552*, 833, 2001.

Mouradian, Z., M. J. Martres, I. Soru-Escaut, and L. Gesztelyi, Local rigid rotation and the emergence of active centers, *Astron. Astrophys.*, *183*, 129–134, 1987.

Ohyama, M., and K. Shibata, X-ray plasma ejections associated with an impulsive flare on 1992 October 5: Physical conditions of X-ray plasma ejection, *Astrophys. J.*, *499*, 934–944, 1998.

Parker, E. N., *Cosmical Magnetic Fields*, Cambridge Univ. Press, New York, 1979.

Pneuman, G. W., The formation of solar prominences by magnetic reconnection and condensation, *Sol. Phys.*, *88*, 219–239, 1983.

Richtmyer, R. O., and K. W. Morton, *Difference Methods for Initial Value Problems*, 2nd ed., chap. 13, Wiley-Interscience, New York, 1967.

Rust, D. M., Magnetic fields in quiescent solar prominences, I, Observations, *Astrophys. J.*, *150*, 313–326, 1967.

Sheeley, N. R., J. H. Walters, Y. M. Wang, and R. A. Howard, Continuous tracking of coronal outflows: Two kinds of coronal mass ejections, *J. Geophys Res.*, *104*, 24,739–24,767, 1999.

Shibata, K., S. Masuda, M. Shimojo, H. Hara, T. Yokoyama, S. Tsuneta, T. Kosugi, and Y. Ogawarai, Hot-plasma ejections associated with compact-loops solar flares, *Astrophys. J. Lett.*, *451*, L83–L85, 1995.

Steinolfson, R. S., Coronal evolution due to shear motion, *Astrophys. J.*, *382*, 677, 1991.

Sterling, A. C., and H. S. Hudson, Yohkoh SXT observations of X-ray "dimming" associated with a halo coronal mass ejection, *Astrophys. J. Lett.*, *491*, L55, 1997.

Stone, J. M., and M. L. Norman, ZEUS-2D: A radiation magnetohydrodynamics code for astrophysical flows in two space dimensions, I, The hydrodynamic algorithms and test, *Astrophys. J. Suppl.*, *80*, 753–790, 1992a.

Stone, J. M., and M. L. Norman, ZEUS-2D: A radiation magnetohydrodynamics code for astrophysical flows in two space dimensions, II, The magnetohydrodynamic algorithms and tests, *Astrophys. J. Suppl.*, *80*, 791–818, 1992b.

Strous, L. H., G. Scharmer, T. D. Tarbell, A. M. Title, and C. Zwaan, Phenomena in an emerging active region, I, Horizontal dynamics, *Astron. Astrophys.*, *306*, 947–959, 1996.

Sturrock, P. A., Maximum energy of semi-infinite magnetic configurations, *Astrophys. J.*, *380*, 655, 1991.

Subramanian, P., K. P. Dere, N. B. Rich, and R. A. Howard, The relationship of coronal mass ejections to streamers, *J. Geophys. Res.*, *104*, 22,321–22,330, 1999.

Van Ballegooijen, A. A., and P. C. H. Martens, Magnetic fields in quiescent prominences, *Astrophys. J.*, *361*, 283–289, 1990.

Wang, H., Evolution of vector magnetic fields and the August 27 1990 X-3 flare, *Sol. Phys.*, *140*, 85, 1992.

Wolfson, R., Equilibria and stability of coronal magnetic arcades, *Astrophys. J.*, *255*, 774, 1982.

Wolfson, R., Shear-induced opening of the coronal magnetic field, *Astrophys. J.*, *443*, 810, 1995.

Zirin, H., Evidence for magnetic field rearrangement in a solar flare, *Astrophys. J.*, *281*, 884–885, 1984.

Zirin, H., and K. Tanaka, Magnetic transients in flares, *Astrophys. J.*, *250*, 791, 1981.

W. B. Manchester IV, Department of Atmospheric and Oceanic Sciences, University of Michigan, Ann Arbor, MI 48109, USA. (chipm@umich.edu)